

Determination of semiconductor band gap state parameters from photoconductivity measurements. I. Theoretical developments

C. Longeaud,¹ J. A. Schmidt,² and J. P. Kleider¹¹*Laboratoire de Génie Electrique de Paris, (UMR 8507 CNRS) Ecole Supérieure d'Electricité, Université Paris VI et XI, Plateau de Moulon, 91192 Gif-sur-Yvette CEDEX, France*²*INTEC (UNL-CONICET), Güemes 3450, and FIQ (UNL), Santiago del Estero 2829, 3000 Santa Fe, Argentina*

(Received 11 October 2005; published 9 June 2006)

In this paper we examine and cross-check the information that can be extracted from different photoconductivity experiments. First, taking account of localized states in the band gap of a semiconductor, we give an analytical expression for the coefficient γ that relates the dc photoconductivity σ to the generation rate G by $\gamma = \delta \ln(\sigma) / \delta \ln(G)$. We demonstrate that in the very simple case when all the gap states have the same capture cross section, it is possible to perform a density of states spectroscopy from the variation of γ with temperature and/or generation rate. We also propose a simplified expression for γ in the case when different species of states are present within the gap of the semiconductor. Second, we put into evidence the links existing between three techniques apparently very different: the dc photoconductivity, the steady-state photocarrier grating, and the modulated photocurrent techniques. The links between the results of these three techniques are explained and illustrated by means of numerical simulations. Finally, we show that the density of states distribution, the capture cross sections of the states, and to a smaller extent, the extended-states mobility of photoconductive semiconductors can be obtained from the comparison of the results of these techniques.

DOI: [10.1103/PhysRevB.73.235316](https://doi.org/10.1103/PhysRevB.73.235316)

PACS number(s): 73.50.-h, 73.61.Jc, 73.50.Pz

I. INTRODUCTION

Except for very pure single crystalline semiconductors, a significant density of defect states is known to exist within the forbidden gap of these materials. These localized states have a major influence on the optoelectronic properties of the semiconductor, providing efficient recombination centers which determine the electrical transport properties and the photoconductivity. It is thus not surprising that several methods have been proposed to probe the density of states (DOS) as a function of energy. In this work we will concentrate on three of these methods, namely the modulated photoconductivity (MPC), the steady-state photocarrier grating (SSPG), and the steady-state photoconductivity (SSPC).

The MPC technique, proposed by Oheda,¹ has proved to be a powerful and convenient method to study the DOS distribution of amorphous and crystalline intrinsic semiconductors. In this experiment the sample is illuminated by a steady flux of light slightly modulated at a pulsation ω . The modulus of the resulting ac current, as well as the phase shift of this current referred to the excitation, are recorded and used to extract information on the DOS. In previous publications we have shown that two regimes have to be considered: the “high-frequency” (MPC-HF) regime^{2,3} and the “low-frequency” (MPC-LF) regime.^{4,5}

The SSPG technique was introduced in 1986 by Ritter *et al.*⁶ to measure the ambipolar diffusion length (L_{amb}) of low-mobility semiconductors. Balberg and co-workers applied the SSPG method in conjunction with steady-state photoconductivity to estimate the DOS of amorphous^{7,8} and microcrystalline silicon⁹ by means of computer simulations based on a presuggested DOS. More recently, we have proposed a procedure to obtain the DOS directly from the application of an explicit reconstruction formula to SSPG measurements.¹⁰ We have analytically solved the generalized equations de-

scribing charge transport and recombination under grating conditions, and we have applied suitable simplifying assumptions to achieve a DOS spectroscopy.¹¹

The SSPC is one of the most widely studied properties of semiconductors. A good deal of theoretical work has been devoted to explain the dependence of the photoconductivity upon temperature or light flux, with the aim to derive defect parameters of the material. Experimentally, for different semiconductors such as CdS, Sb₂S₃, or hydrogenated amorphous silicon (a-Si:H), a power-law dependence of the photoconductivity σ on the light flux F has been observed, $\sigma \propto F^\gamma$. For a-Si:H in particular, two prominent features that characterize its photoconductivity are the thermal quenching, i.e., the decrease of σ with temperature over a limited temperature range, and the superlinearity of γ values, i.e., $\gamma > 1$ over the same temperature range where the thermal quenching takes place. These phenomena, also observed in some crystalline semiconductors, have been explained by Rose¹² as due to a change in the recombination channel between two defect states with different capture coefficients—a process known as sensitization. The Rose model also provided explicit dependence of γ with the temperature and the DOS, showing that in an exponentially varying DOS—for instance, the conduction band tail of a-Si:H—the exponent would be given by $\gamma = T_c / (T + T_c)$, where T is the temperature and T_c the characteristic temperature that describes the exponentially decreasing conduction band tail. Following this pioneering work, several authors explored the connection between the γ exponent and the DOS. Liu and Wagner¹³ provided a simple analytical expression for the γ coefficient in the case of a known DOS, and Mendoza and Pickin¹⁴ were able to deduce an explicit formula to get the DOS at the electron quasi-Fermi level from γ measurements. These authors, however, neglected in their treatment the holes contribution and restricted their analysis to a single species of

monovalent gap states. More comprehensive model-simulation studies have been developed by Tran¹⁵ as well as Shen and Wagner,¹⁶ who successfully reproduced the experimentally observed thermal quenching of the photoconductivity and superlinearity of γ . However, these complete models could only be treated through numerical calculations, and no analytical expression for γ as a function of the DOS parameters has been provided by these authors.

In this work we give an analytical expression for γ valid for an arbitrary DOS distribution, and under certain approximations we propose a very simple formula relating the DOS at the electron quasi-Fermi level to experimental quantities. In Sec. II we present the calculation from which we deduce the analytical expression for γ . It is shown in Sec. III how this expression can lead, under some conditions, to the determination of the DOS of the semiconductor. This calculation is compared in Sec. IV to previous calculations made to determine the DOS from either MPC or SSPG techniques. In Sec. V we illustrate these calculations and experimental results by means of simulations that show how some of the parameters of the DOS can be deduced from SSPC measurements associated with other techniques, and finally we conclude in Sec. VI.

II. CALCULATION OF γ

Let us consider an intrinsic semiconductor containing m species of monovalent states within the gap. The species—or classes—of states were defined by Simmons and Taylor¹⁷ according to their respective capture coefficients for electrons (C_n^i) and holes (C_p^i), with $1 \leq i \leq m$. For this semiconductor, enlightened by a uniformly absorbed dc light flux creating free carriers by band-to-band generation, the continuity and charge neutrality equations can be written

$$\frac{\partial n}{\partial t} = G - \sum_1^m \int_{E_v}^{E_c} [\bar{n}^i(1-f^i) - e_n^i f^i] N^i dE + \frac{1}{q} \text{div}(J_n), \quad (1)$$

$$\frac{\partial p}{\partial t} = G - \sum_1^m \int_{E_v}^{E_c} [\bar{p}^i f^i - e_p^i(1-f^i)] N^i dE - \frac{1}{q} \text{div}(J_p), \quad (2)$$

$$\text{div}(\xi) = \frac{q}{\varepsilon} \left[p - p_0 - (n - n_0) - \sum_1^m \int_{E_v}^{E_c} N^i (f^i - f_0) dE \right]. \quad (3)$$

In these equations, n (p) is the density of electrons (holes) in the extended states (n_0 and p_0 being the values under dark equilibrium conditions), $\bar{n}^i = n C_n^i$ ($\bar{p}^i = p C_p^i$) is the capture rates of electrons (holes) from the i th species of trap, e_n^i (e_p^i) is the energy-dependent emission rates of electrons (holes) from the i th species of trap, J_n (J_p) is the current density of electrons (holes), G is the band-to-band generation rate, ε is the dielectric constant, q is the absolute value of the electron charge, ξ is the applied electric field between both electrodes, N^i is the density of states of species i , f^i is the occupation function of the i th species of trap under illumination, and f_0 is the occupation functions under dark equilibrium (the same

for all the traps). In our analysis we consider only band-to-band generation, neglecting optical transitions involving localized states due to their much lower probability.

In these equations some quantities are energy dependent and some are not. The densities of states N^i , the occupation functions f^i , and the emission rates of electrons and holes e_n^i and e_p^i are all energy-dependent quantities, but to lighten the equations we have omitted the (E) for all of them. We have assumed that the capture coefficients C_n^i and C_p^i do not depend on energy. The relation between the emission rates and the capture coefficients is given by a detailed balance study of the exchange of carriers under thermal equilibrium conditions, between the extended states and a trapping level at energy E , leading to

$$e_n^i = C_n^i N_c \exp\left(-\frac{E_c - E}{k_B T}\right), e_p^i = C_p^i N_v \exp\left(-\frac{E - E_v}{k_B T}\right),$$

k_B being the Boltzmann constant, T the absolute temperature, and N_c (N_v) the equivalent densities of states at the bottom (top) of the conduction (valence) band. Under nonequilibrium, we make the usual assumption that the capture and emission rates remain unaltered with respect to equilibrium conditions.

As a matter of simplification, considering uniform and steady-state illumination and ohmic contacts, we can assume that $\partial n / \partial t = 0$, $\partial p / \partial t = 0$, $\text{div}(J) = 0$, and $\text{div}(\xi) = 0$. The expression for f^i is

$$f^i(E) = [\bar{n}^i + e_p^i(E)] \tau^i(E),$$

with

$$\tau^i(E) = \frac{1}{\bar{n}^i + \bar{p}^i + e_n^i(E) + e_p^i(E)}. \quad (4)$$

From the continuity Eq. (1), the electron (hole) lifetime τ_n (τ_p) can be defined. Indeed, a very simple calculation leads to

$$G = \sum_1^m \int_{E_v}^{E_c} (\bar{n}^i \bar{p}^i - e_n^i e_p^i) \tau^i N^i dE, \quad (5)$$

where the product $e_n^i e_p^i$ can be neglected.¹⁸ Thus, writing $G = n / \tau_n$ or $G = p / \tau_p$, one ends with

$$\frac{1}{\tau_n} = \sum_1^m C_n^i \bar{p}^i \int_{E_v}^{E_c} \tau^i N^i dE$$

and

$$\frac{1}{\tau_p} = \sum_1^m C_p^i \bar{n}^i \int_{E_v}^{E_c} \tau^i N^i dE. \quad (6)$$

Before calculating an expression of γ we present in Fig. 1 an example of the states occupancy under dark equilibrium and under steady-state illumination. In Fig. 1(a) we present a DOS that could be representative of hydrogenated amorphous silicon, with two band tails and Gaussian-shaped deep

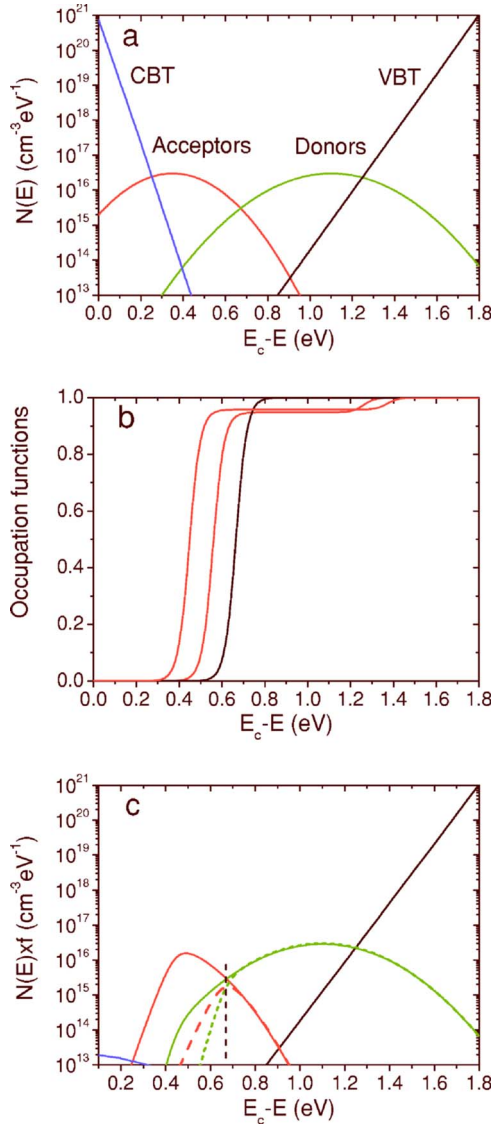


FIG. 1. (Color online) (a) Density of states typical of hydrogenated amorphous silicon. (b) Plots of different occupation functions vs energy under dark equilibrium and for different light fluxes (10^{13} and $10^{15} \text{ cm}^{-2} \text{ s}^{-1}$), from right to left of the figure. The occupation functions depart from 0 at a lower energy with increasing flux. (c) The states occupancy $[N(E) \times f(E)]$ under dark (dashed lines) and under a $10^{15} \text{ cm}^{-2} \text{ s}^{-1}$ flux (full lines). The energy position of the dark Fermi level is shown by the vertical dashed line.

defect densities. Note that the energy scaling is referenced to E_c . For simplicity all the states have been given the same capture coefficients for holes and electrons, so that we will have to deal with a single occupation function under illumination ($i=1$). We present the occupation functions under dark and under two different fluxes of 10^{13} and $10^{15} \text{ cm}^{-2} \text{ s}^{-1}$ (curves from right to left, respectively) in Fig. 1(b), and the resulting states occupancy [i.e., the product $N(E) \times f(E)$] under dark (dashed lines) and for the highest flux (full lines) in Fig. 1(c). These figures are the results of numerical simulations described and used in more details in Sec. V. The occupation function under dark is calculated from the determi-

nation of the electrical neutrality [Eq. (3) with $\text{div}(\xi)=0$], assuming that the valence band tail states are of donor type (neutral when filled) and the conduction band tail states are of acceptor type (neutral when empty). We deduce from this calculation the dark Fermi level energy position E_f [vertical dashed line in Fig. 1(c)] and the extended-states density of electrons and holes, n_0 and p_0 , respectively. Under dark equilibrium the occupation function is a one-step function, roughly speaking equal to 0 for $E < E_f$ and to 1 for $E > E_f$. Under illumination, the density of carriers in the extended states and the occupation function [given by Eq. (4)] are calculated from the numerical resolution of the electrical neutrality [Eq. (3) with $\text{div}(\xi)=0$] and one of the two continuity [Eqs. (1) and (2)] equations. A typical shape of $f(E)$ is a two-step function [Fig. 1(b)], where the energy extent of the middle step around E_f depends on the light flux. It can be seen in Fig. 1(c) that the acceptor states located above E_f are partially filled when the flux increases from 0 to $10^{15} \text{ cm}^{-2} \text{ s}^{-1}$. Note also that the conduction band tail states are always almost empty. A significant filling, though probably partial, of these states would need a very high flux, at least in the present example. This illustration is in complete agreement with the detailed study presented years ago by Simmons and Taylor,¹⁷ which is why we will not enter into further details.

To calculate γ we will assume that the applied flux is made of a main component plus a small perturbation. To the first order, most of the quantities Q appearing in Eqs. (1)–(3) can be written as $Q_0 + \delta Q$. From a logarithmic derivative, one can deduce the expression of δf^i

$$\delta f^i = f^i \left(\frac{\delta \bar{n}^i}{\bar{n}^i + e_p^i} - \frac{\delta \bar{p}^i + \delta p^i}{\bar{n}^i + \bar{p}^i + e_n^i + e_p^i} \right). \quad (7)$$

Introduction of Eq. (7) into Eqs. (1)–(3) gives, for the continuity equations,

$$0 = \delta G - \delta n \sum_1^m \int C_n^i (1 - f^i) (\bar{p}^i + e_p^i) \tau^i N^i dE - \delta p \sum_1^m \int C_p^i f^i (\bar{n}^i + e_n^i) \tau^i N^i dE, \quad (8)$$

and for the charge neutrality equation

$$\delta n \left[1 + \sum_1^m C_n^i \int N^i (1 - f^i) \tau^i dE \right] = \delta p \left(1 + \sum_1^m C_p^i \int N^i f^i \tau^i dE \right), \quad (9)$$

where the integrals are taken from E_v to E_c . Replacement of Eq. (9) into Eq. (8) gives

$$\delta G = \frac{\delta p}{\tau_p'} = \frac{\delta n}{\tau_n'}, \quad (10)$$

where

$$\frac{1}{\tau'_n} = \sum_1^m C_n^i \int (1-f^i)(\bar{p}^i + e_p^i) \tau^i N^i dE + \sum_1^m C_p^i \int f^i(\bar{n}^i + e_n^i) \tau^i N^i dE \frac{\left[1 + \sum_1^m C_n^i \int (1-f^i) \tau^i N^i dE \right]}{\left(1 + \sum_1^m C_p^i \int f^i \tau^i N^i dE \right)}, \quad (11)$$

and

$$\frac{1}{\tau'_p} = \sum_1^m C_p^i \int f^i(\bar{n}^i + e_n^i) \tau^i N^i dE + \sum_1^m C_n^i \int (1-f^i)(\bar{p}^i + e_p^i) \tau^i N^i dE \frac{\left(1 + \sum_1^m C_p^i \int f^i \tau^i N^i dE \right)}{\left[1 + \sum_1^m C_n^i \int (1-f^i) \tau^i N^i dE \right]}. \quad (12)$$

These two quantities, τ'_n and τ'_p , can be considered as the lifetime of the excess carriers created by the excess generation rate δG , and they are different from the electron and hole lifetimes defined in Eq. (6).

Introducing the photoconductivity σ and the electron (hole) extended-states mobility μ_n (μ_p), we define the factor γ by $\gamma = \delta \ln(\sigma) / \delta \ln(G)$ and we can write

$$\gamma \frac{\delta G}{G} = \frac{\delta \sigma}{\sigma} = \frac{q\mu_n \delta n + q\mu_p \delta p}{q(\mu_n \tau_n + \mu_p \tau_p) G} = \frac{\mu_n \tau'_n + \mu_p \tau'_p}{\mu_n \tau_n + \mu_p \tau_p} \frac{\delta G}{G}, \quad (13)$$

which, from the above equations, gives a general expression for γ ,

$$\gamma = \frac{\frac{1}{(\mu_n \tau_n + \mu_p \tau_p)} \left[\mu_n \left(1 + \sum_1^m C_p^i \int f^i \tau^i N^i dE \right) + \mu_p \left(1 + \sum_1^m C_n^i \int (1-f^i) \tau^i N^i dE \right) \right]}{\sum_1^m C_n^i \int (1-f^i)(\bar{p}^i + e_p^i) \tau^i N^i dE \left(1 + \sum_1^m C_p^i \int f^i \tau^i N^i dE \right) + \sum_1^m C_p^i \int f^i(\bar{n}^i + e_n^i) \tau^i N^i dE \left(1 + \sum_1^m C_n^i \int (1-f^i) \tau^i N^i dE \right)}. \quad (14)$$

We shall try to simplify Eq. (14) to obtain more information, especially on the DOS. If we neglect the 1 in the parenthesis $(1 + \sum_1^m C_p^i \int f^i \tau^i N^i dE)$ and $(1 + \sum_1^m C_n^i \int (1-f^i) \tau^i N^i dE)$, which is equivalent to assuming that charge neutrality is mainly controlled by trapped carriers rather than by free carriers (as usual in defective semiconductors), and if we multiply by np the numerator and denominator of Eq. (14), we obtain

$$\gamma = \frac{\frac{G}{(\mu_n \tau_n + \mu_p \tau_p)} \left[\mu_n \tau_n \sum_1^m \bar{p}^i \int f^i \tau^i N^i dE + \mu_p \tau_p \sum_1^m \bar{n}^i \int (1-f^i) \tau^i N^i dE \right]}{\sum_1^m \bar{n}^i \int (1-f^i)(\bar{p}^i + e_p^i) \tau^i N^i dE \sum_1^m \bar{p}^i \int f^i \tau^i N^i dE + \sum_1^m \bar{p}^i \int f^i(\bar{n}^i + e_n^i) \tau^i N^i dE \sum_1^m \bar{n}^i \int (1-f^i) \tau^i N^i dE}. \quad (15)$$

To simplify the expression (15) we define the coefficients A_n , A_p , B_n , and B_p by

$$\begin{aligned}
 & \sum_1^m \bar{p}^i \int f^i \tau^i N^i dE \\
 &= \sum_1^m \int \bar{p}^i \bar{n}^i \tau^i N^i dE \left[1 + \frac{\sum_1^m \int \bar{p}^i e_p^i \tau^i N^i dE}{\sum_1^m \int \bar{p}^i \bar{n}^i \tau^i N^i dE} \right] \\
 &= \sum_1^m \int \bar{p}^i \bar{n}^i \tau^i N^i dE [1 + A_p], \tag{16}
 \end{aligned}$$

$$\begin{aligned}
 & \sum_1^m \bar{n}^i \int (1 - f^i) (\bar{p}^i + e_p^i) \tau^i N^i dE \\
 &= \sum_1^m \bar{n}^i \bar{p}^i \int \tau^i N^i dE - \sum_1^m \bar{n}^i \bar{p}^i \int \tau^i N^i dE \\
 &= G - \sum_1^m \bar{n}^i \bar{p}^i \int \tau^i N^i dE = G(1 - B_n), \tag{18}
 \end{aligned}$$

and,

$$\begin{aligned}
 & \sum_1^m \bar{n}^i \int (1 - f^i) \tau^i N^i dE \\
 &= \sum_1^m \int \bar{p}^i \bar{n}^i \tau^i N^i dE \left[1 + \frac{\sum_1^m \int \bar{n}^i e_n^i \tau^i N^i dE}{\sum_1^m \int \bar{p}^i \bar{n}^i \tau^i N^i dE} \right] \\
 &= \sum_1^m \int \bar{p}^i \bar{n}^i \tau^i N^i dE [1 + A_n], \tag{17}
 \end{aligned}$$

$$\begin{aligned}
 & \sum_1^m \bar{p}^i \int f^i (\bar{n}^i + e_n^i) \tau^i N^i dE \\
 &= \sum_1^m \bar{n}^i \bar{p}^i \int \tau^i N^i dE - \sum_1^m \bar{n}^i \bar{p}^i \int \tau^i N^i dE \\
 &= G - \sum_1^m \bar{n}^i \bar{p}^i \int \tau^i N^i dE = G(1 - B_p). \tag{19}
 \end{aligned}$$

 Using these simplified notations— A_n , A_p , B_n , and B_p —one finally ends with

$$\frac{1}{\gamma} - 1 = \frac{[1 + A_p] \left[1 - B_n - \frac{\mu_n \tau_n}{\mu_n \tau_n + \mu_p \tau_p} \right] + [1 + A_n] \left[1 - B_p - \frac{\mu_p \tau_p}{\mu_n \tau_n + \mu_p \tau_p} \right]}{\frac{\mu_n \tau_n}{\mu_n \tau_n + \mu_p \tau_p} [1 + A_p] + \frac{\mu_p \tau_p}{\mu_n \tau_n + \mu_p \tau_p} [1 + A_n]}. \tag{20}$$

Note that, apart from the assumption that the electrical neutrality is mostly controlled by trapped carriers, up to here there is no approximation.

To go further, i.e., to extract some information on the DOS, we have simplified A_n , A_p , B_n , and B_p with approximations already used in other calculations.^{5,11} For instance, the integral appearing in Eq. (17) can be simplified as

$$\begin{aligned}
 & C_n^i \int_{E_v}^{E_c} (1 - f^i) \tau^i N^i dE \\
 &\approx C_p^i C_n^i p \int_{E_{ip}^i}^{E_{in}^i} (\tau^i)^2 N^i dE \\
 &\quad + C_n^i \int_{E_v}^{E_c} e_n^i (\tau^i)^2 N^i dE \\
 &\approx \tau_t^i \left(C_n^i C_p^i p \tau_t^i \int_{E_{ip}^i}^{E_{in}^i} N^i dE + C_n^i N_n^i \right)
 \end{aligned}$$

$$\approx \tau_t^i \left(\frac{1}{\tau_j^i} + C_n^i N_n^i \right), \tag{21}$$

where τ_n^i is the electron “lifetime” for this species of states [see Eq. (6)], such that $1/\tau_n = \sum_1^m 1/\tau_n^i$, τ_t^i is given by

$$\tau_t^i = \frac{1}{C_n^i n + C_p^i p} = \frac{1}{G(C_n^i \tau_n + C_p^i \tau_p)}, \tag{22}$$

and $N_n^i = k_B T N(E_{in}^i)$, $N(E_{in}^i)$ being the density of states at the quasi-Fermi level (E_{in}^i) for electrons trapped in the i th species of states. We will also call τ_p^i the hole “lifetime” for this species of states [Eq. (6)] and $N_p^i = k_B T N(E_{ip}^i)$, $N(E_{ip}^i)$ being the density of states at the quasi-Fermi level (E_{ip}^i) for trapped holes. With these approximation we can write

$$A_n = \frac{\sum_1^m \bar{n}^i \tau_t^i N_n^i}{\sum_1^m \bar{p}^i \bar{n}^i \tau_t^i \int_{E_{ip}^i}^{E_{in}^i} N^i dE}, \quad A_p = \frac{\sum_1^m \bar{p}^i \tau_t^i N_p^i}{\sum_1^m \bar{p}^i \bar{n}^i \tau_t^i \int_{E_{ip}^i}^{E_{in}^i} N^i dE},$$

$$B_n = \frac{\sum_1^m \bar{p}^i \bar{n}^i (\tau_i^j)^2 \int_{E_{ip}^i}^{E_m^i} N^i dE}{G}, \quad B_p = \frac{\sum_1^m \bar{p}^i \bar{n}^i (\tau_i^j)^2 \int_{E_{ip}^i}^{E_m^i} N^i dE}{G}, \quad (23)$$

where the integrals are now taken from E_{ip}^i to E_m^i . Note that these approximate expressions have to be used with caution. Indeed, by using Eqs. (23) one would obtain $1 - B_n - B_p = 0$, whereas the correct expression is

$$1 - B_n - B_p = \frac{1}{G} \sum_1^m \int_{E_v}^{E_c} \bar{n}^i \bar{p}^i (e_n^i + e_p^i) N^i (\tau_i^j)^2 dE. \quad (24)$$

As we will see below, this quantity may have some influence on the final calculation.

III. DETERMINATION OF THE DENSITY OF STATES

A. One species of states

Before dealing with the case of one species of states, let us modify slightly expression (20), which can be written

$$\frac{1}{\gamma} - 1 = \frac{A_p \left[1 - B_n - \frac{\mu_n \tau_n}{\mu_n \tau_n + \mu_p \tau_p} \right] + A_n \left[1 - B_p - \frac{\mu_p \tau_p}{\mu_n \tau_n + \mu_p \tau_p} \right] + 1 - B_n - B_p}{\frac{\mu_n \tau_n}{\mu_n \tau_n + \mu_p \tau_p} [1 + A_p] + \frac{\mu_p \tau_p}{\mu_n \tau_n + \mu_p \tau_p} [1 + A_n]}. \quad (25)$$

If we consider only one species of states, using expressions (23) and (24), the first order approximations for the coefficients are

$$A_n = C_n \tau_n N_n; \quad A_p = C_p \tau_p N_p; \quad B_n = C_n n \tau_i; \quad B_p = C_p p \tau_i; \\ \text{and} \quad 1 - B_n - B_p \approx A_n \bar{p} \tau_i + A_p \bar{n} \tau_i.$$

For a semiconductor where electrons are the majority carriers, such that $\mu_n \tau_n \gg \mu_p \tau_p$, then we easily obtain

$$\frac{1}{\gamma} - 1 = \frac{A_n}{1 + A_p}. \quad (26)$$

Assuming that the denominator is almost equal to 1 (a reasonable assumption if the holes contribution is negligible), Eq. (26) transforms into

$$\frac{N(E_m) C_n}{\mu_n} = \frac{G}{k_B T \mu_n n} \left(\frac{1}{\gamma} - 1 \right) = \frac{qG}{k_B T \sigma} \left(\frac{1}{\gamma} - 1 \right). \quad (27)$$

Since the electrons are the majority carriers, $E_m \approx E_{fn}$, E_{fn} being the quasi-Fermi level for free electrons under illumination. The energy position can be readily calculated from the photocurrent value as

$$E_c - E_{fn} = k_B T \ln \left(\frac{S q \xi \mu_n N_c}{I_{ph}} \right), \quad (28)$$

where S is the conduction cross-sectional area in which the photocurrent I_{ph} is flowing and N_c the equivalent density of states at the bottom of the conduction band.

Equations (27) and (28) are the basic ones that allow us to use the evolution of γ with flux and/or with temperature to perform a spectroscopic evaluation of the DOS interacting with free electrons. If we considered the case where holes were the majority carriers ($\mu_p \tau_p \gg \mu_n \tau_n$), we would obtain expressions similar to Eqs. (27) and (28), replacing all the n 's by p 's, $E_c - E_{fn}$ by $E_{fp} - E_v$, and N_c by N_v (the equivalent density of states at the top of the valence band). The spectroscopy would be that of the DOS interacting with free holes.

B. Different species of states

If one considers a material for which $\mu_n \tau_n \gg \mu_p \tau_p$, Eq. (24) leads to

$$\frac{1}{\gamma} - 1 = \frac{-A_p B_n + A_n (1 - B_p) + (1 - B_n - B_p)}{(1 + A_p)} = \frac{\text{Num}}{\text{Den}}.$$

Replacing Eqs. (16)–(19) into this expression leads to

$$\text{Num} = \frac{-\sum_1^m \int \bar{p}^i e_p^i \tau^i N^i dE \sum_1^m \int \bar{n}^i \bar{p}^i \tau^i N^i dE + \sum_1^m \int \bar{n}^i e_n^i \tau^i N^i dE \sum_1^m \int \bar{p}^i (\bar{n}^i + e_p^i) (\bar{n}^i + e_n^i) \tau^i N^i dE}{G \sum_1^m \int \bar{p}^i \bar{n}^i \tau^i N^i dE} + \frac{1}{G} \sum_1^m \int_{E_v}^{E_c} \bar{n}^i \bar{p}^i (e_n^i + e_p^i) \tau^i N^i dE. \quad (29)$$

The terms containing products of the emission rates can be neglected in front of those terms containing integrals of the DOS between E_{tp}^i and E_m^i . With these approximations Eq. (29) transforms into

$$\text{Num} = \frac{\sum_1^m \int \bar{n}^i \bar{p}^i \tau^i N^i dE \left[\sum_1^m \int \bar{n}^i e_n^i \tau^i N^i dE - \sum_1^m \int \bar{p}^i e_p^i \tau^i N^i dE \right]}{G \sum_1^m \int \bar{p}^i \bar{n}^i \tau^i N^i dE} + \frac{1}{G} \sum_1^m \int_{E_v}^{E_c} \bar{n}^i \bar{p}^i (e_n^i + e_p^i) \tau^i N^i dE. \quad (30)$$

If we write

$$G^i = \frac{\bar{n}^i \bar{p}^i}{\bar{n}^i + \bar{p}^i} \int_{E_{tp}^i}^{E_m^i} N^i dE = \bar{n}^i \bar{p}^i \tau_t^i \int_{E_{tp}^i}^{E_m^i} N^i dE = \frac{n}{\tau_n^i}, \quad (31)$$

then, with the usual approximate expressions, we get

$$\text{Num} = \frac{\sum_{i=1}^m \left[\bar{n}^i N_n^i \tau_t^i \times \sum_{j=1}^m G^j \tau_t^j (\bar{p}^j + \bar{n}^j) \right] + \sum_{i=1}^m \left[\bar{p}^i N_p^i \tau_t^i \times \sum_{j=1}^m G^j \tau_t^j (\bar{n}^i - \bar{n}^j) \right]}{G \sum_{i=1}^m G^i \tau_t^i}. \quad (32)$$

To further simplify this expression, one has to make more assumptions. A great simplification arises if one assumes that the holes contribution can be fully neglected. In this case one ends with

$$\frac{1}{\gamma} - 1 = \frac{\sum_{i=1}^m N_n^i}{\sum_{i=1}^m G_i \tau_t^i} = \frac{\tau_n \sum_{i=1}^m N_n^i}{\tau_n \sum_{i=1}^m \frac{1}{C_n^i \tau_n^i}}, \quad (33)$$

from which the density of states cannot be directly deduced but, as we will see later, some interesting information can be extracted. The denominator of the right-hand side of Eq. (33) can be considered as the reciprocal of an average value of the capture coefficient of the recombining states. In some cases, as we will see later, this denominator can be equal to the reciprocal of the capture coefficient of the *dominant* recombining state, and the term on the right-hand side of Eq. (33) can be compared to the coefficient A_n defined in the case of a single species of states.

Of course, the drastic approximation of fully neglecting the holes contribution may not always be valid, and even for the same material it may depend on the experimental condi-

tions. Note that the holes term that we have neglected in Eq. (32) to obtain Eq. (33) can be negative. If this term turns out to be predominant, it means that γ will be larger than 1. This “superlinear” behavior of γ , usually explained in terms of a sensitization effect, is often met in a-Si:H, especially at low temperatures.

To illustrate and clarify the calculations developed above we have used numerical simulations, examples of which will be presented in Sec. V. Prior to that, we would like to show that links between the above calculations and previous developments concerning other experimental methods can be drawn.

IV. COMPARISON WITH OTHER EXPERIMENTS

In this section we will show that the above calculation can be linked to previous calculations developed for the SSPG and MPC techniques. However, for this purpose we will only consider a single type of state because our previous calculations on SSPG and MPC were done under this assumption.

A. The steady-state photocarrier grating technique

The SSPG experiment was proposed in 1986 to determine the ambipolar diffusion length of the minority carriers.⁶

Many laboratories have adopted this technique, particularly well suited for material presenting a small diffusion length, and several works concerning this technique and its validity have been published. The basis of the experiment consists of illuminating the part of the sample located between two coplanar electrodes with two laser beams having an angle θ between them, an intense one of intensity I_1 and another one attenuated to a smaller intensity I_2 . If the two beams are coherent and have the same polarization, a light grating develops between the two electrodes with an intensity

$$I(x) = I_1 + I_2 + \gamma_0 2\sqrt{I_1 I_2} \cos\left(\frac{2\pi x}{\Lambda}\right),$$

where x is the space coordinate perpendicular to the electrodes, γ_0 is a factor taking account of the quality of the interferences ($0 < \gamma_0 \leq 1$), and Λ is the grating period (dependent on θ). When the two beams have perpendicular polarizations and do not interfere, the light intensity impinging on the sample is simply $I_0 = I_1 + I_2$, giving rise to a generation rate $G_0 = G_1 + G_2$, and the current density flowing through the sample under the applied electric field is j_0 . In practice the less intense beam is chopped at a low frequency and one measures the resulting current by means of a lock-in amplifier. When the two beams do not interfere, the signal detected by the lock-in amplifier is proportional to $j_{woi} = j_0 - j_1$, j_1 being the current created by the illumination of the intense beam (I_1) alone. When a light grating is developed on the sample, the signal detected by the lock-in amplifier is $j_{wi} = j_0 - j_1 + \Delta j$. In the standard SSPG experiment the ambipolar diffusion length is deduced from the evolution of $\beta = j_{wi}/j_{woi}$ as a function of Λ .

Though the SSPG is usually used, for instance in a-Si:H, to derive information on the *minority* carriers, in recent publications we have shown that it is possible to deduce some part of the DOS distribution interacting with the *majority* carriers, from the value of β taken at large grating periods.^{10,11} We show in the following that a link can be drawn between this previous result and the present calculations.

According to our previous publications,^{10,11} the expression of the excess current density Δj when a light grating is developed onto the sample is

$$\Delta j = -\frac{q^2 \Delta G^2}{2\varepsilon \tau_d} \frac{\xi}{DEN} \times \left[\mu_n C_p \int f \tau N dE + \mu_p C_n \int (1-f) \tau N dE \right], \quad (34)$$

where τ_d is the dielectric relaxation time and $\Delta G = 2\gamma_0 \sqrt{G_1 G_2}$. To give the expression of DEN , we assume that the applied electric field is low, so that the terms involving the field contribution can be neglected (for low electric field regime, see Ref. 11 and references therein). We will also write

$$D_\gamma = \int C_n (1-f)(\bar{p} + e_p) \tau N dE \left(1 + C_p \int f \tau N dE \right) + \int C_p f(\bar{n} + e_n) \tau N dE \left(1 + C_n \int (1-f) \tau N dE \right), \quad (35)$$

with D_γ being simply the denominator of γ in the case of a single species of states [see Eq. (14)]. We then have

$$DEN = \frac{D_\gamma^2}{\tau_d^2} \left[1 + k^2 L_n^2 \frac{\tau_d}{\tau_n} \int C_p f(\bar{n} + e_n) \tau N dE + k^2 L_p^2 \frac{\tau_d}{\tau_p} \int C_n (1-f)(\bar{p} + e_p) \tau N dE + \mu \tau_a K \left(\frac{\tau'_p}{\tau_p} + \frac{\tau'_n}{\tau_n} \right) + k^4 \frac{L_n^2 L_p^2 \tau_d}{D \tau_n \tau_p} \right]^2, \quad (36)$$

where $\mu \tau_a = (\mu_n \tau_n \times \mu_p \tau_p) / (\mu_n \tau_n + \mu_p \tau_p)$ and $K = k^2 k_B T / q$ with $k = 2\pi/\Lambda$. In the limit of large grating periods ($\Lambda \rightarrow \infty$), DEN is simply equal to D_γ^2 / τ_d^2 and the expression of Δj becomes

$$\Delta j_{\text{lim}} = -\frac{1}{2} \frac{\Delta G^2}{G_0^2} \gamma^2 j_0. \quad (37)$$

The expression of β under these conditions is

$$\beta_{\text{lim}} = 1 - \frac{1}{2} \left(\frac{\Delta G}{G_0} \right)^2 \gamma^2 \frac{j_0}{j_0 - j_1}. \quad (38)$$

As far as the currents are concerned, one may write

$$\frac{j_0 - j_1}{j_0} = \frac{\delta \sigma}{\sigma_0} = \gamma \frac{G_2}{G_0}, \quad (39)$$

where σ_0 is the photoconductivity resulting from G_0 , an equation that gives

$$\beta_{\text{lim}} = 1 - \frac{2\gamma \gamma_0^2 G_1}{G_0}. \quad (40)$$

In Ref. 11 we have shown that $N(E_{fn})$ can be deduced from β_{lim} according to

$$N(E_{fn}) = \frac{q \mu_n G_0}{C_n k_B T \sigma_0} \left[\frac{\gamma_0}{(1 + G_2/G_1)} \sqrt{\frac{2(1 + \gamma G_2/G_1)}{\gamma(1 - \beta_{\text{lim}})}} - 1 \right]. \quad (41)$$

Injecting Eq. (40) into Eq. (41) and taking into account that G_2 is usually much lower than G_1 (at least $G_2 = G_1/10$), we obtain

$$\frac{N(E_{fn}) C_n}{\mu_n} = \frac{q G_0}{k_B T \sigma_0} \left(\frac{1}{\gamma} - 1 \right), \quad (42)$$

which is precisely Eq. (27) of the present paper.

In conclusion, the SSPG experiment performed with large gratings should bring the same information on the material as SSPC. We will see that it is actually the case by performing both simulations on the same “sample.”

B. The modulated photocurrent experiment

We have shown in previous works that the modulated photocurrent (MPC) experiment contributed to gain insight into the DOS of different semiconductors.^{2,3,19} In this experiment the sample is illuminated by a steady flux of light slightly modulated at a pulsation ω . The modulus of the ac current I_{ac} resulting from the ac generation rate G_{ac} , as well as the phase shift ϕ between I_{ac} and G_{ac} , are recorded and used to extract information on the DOS. We have shown that two regimes have to be considered, the “high-frequency” (MPC-HF) regime that gives a spectroscopy of the quantity NC/μ , and the “low-frequency” (MPC-LF) regime from which a DOS spectroscopy can be achieved.^{4,5} Of course, these experiments do not reveal the complete DOS but only the part with which the majority carriers are interacting. Each regime brings complementary information on the electronic parameters. The aim of this section is to put into evidence that the data measured by the MPC technique performed in the “low frequency” regime are related to the γ measurements. As mentioned above, we will restrict the present calculation to a single species of states.

For the derivation of the ac photocurrent we start from the expressions (11), (12), and (26)–(29) of a preceding paper.¹⁹ Using the same notations, we have

$$\frac{I_{ac}}{Sq\xi G_{ac}} = \frac{1}{D} \left[\mu_n \left(j\omega + \frac{1}{\tau_{p,p}} - \frac{1}{\tau_{n,p}} \right) + \mu_p \left(j\omega + \frac{1}{\tau_{n,n}} - \frac{1}{\tau_{p,n}} \right) \right], \quad (43)$$

with

$$\frac{1}{\tau_{n,n}} = \frac{1}{\tau_{p,n}} + j\omega C_n \int_{E_V}^{E_C} N(E) \frac{(1-f)}{1/\tau + j\omega} dE, \quad (44)$$

$$\frac{1}{\tau_{p,p}} = \frac{1}{\tau_{n,p}} + j\omega C_p \int_{E_V}^{E_C} N(E) \frac{f}{1/\tau + j\omega} dE, \quad (44)$$

where τ is given by Eq. (4), taking $i=1$, and

$$D = \left(j\omega + \frac{1}{\tau_{n,n}} \right) \left(j\omega + \frac{1}{\tau_{p,p}} \right) - \frac{1}{\tau_{n,p}\tau_{p,n}}. \quad (45)$$

Thus, for $\omega \rightarrow 0$ we obtain

$$\frac{1}{\tau_{n,n}} \frac{1}{\tau_{p,p}} - \frac{1}{\tau_{p,n}} \frac{1}{\tau_{n,p}} \approx j\omega C_n C_p \left[\int_{E_V}^{E_C} N(E) \tau(\bar{p} + e_p)(1-f)dE \int_{E_V}^{E_C} N(E) \tau f dE + \int_{E_V}^{E_C} N(E) \tau(\bar{n} + e_n) f dE \int_{E_V}^{E_C} N(E) \tau(1-f)dE \right], \quad (46)$$

and

$$D \approx j\omega C_n \int_{E_V}^{E_C} N(E) \tau(\bar{p} + e_p)(1-f)dE + j\omega C_p \int_{E_V}^{E_C} N(E) \tau(\bar{n} + e_n) f dE + j\omega C_n C_p \left[\int_{E_V}^{E_C} N(E) \tau(\bar{p} + e_p)(1-f)dE \int_{E_V}^{E_C} N(E) \tau f dE + \int_{E_V}^{E_C} N(E) \tau(\bar{n} + e_n) f dE \int_{E_V}^{E_C} N(E) \tau(1-f)dE \right]. \quad (47)$$

Replacing Eqs. (44)–(47) into Eq. (43), one gets

$$\frac{I_{ac}}{Sq\xi G_{ac}} = \frac{\left[\mu_n C_p \int_{E_V}^{E_C} N f \tau dE + \mu_p C_n \int_{E_V}^{E_C} N(1-f) \tau dE \right]}{\int_{E_V}^{E_C} C_n (1-f)(\bar{p} + e_p) \tau N dE \left(1 + C_p \int_{E_V}^{E_C} N f \tau dE \right) + \int_{E_V}^{E_C} C_p f(\bar{n} + e_n) \tau N dE \left(1 + C_n \int_{E_V}^{E_C} N(1-f) \tau dE \right)}. \quad (48)$$

If one neglects the 1 in the large brackets of the denominator, which is equivalent to assume that trapped carriers are much more numerous than free carriers, and multiplies by np the numerator and denominator of the previous expression, one can write

$$\frac{I_{ac}}{Sq\xi G_{ac}} = \frac{\frac{G}{\mu_n\tau_n + \mu_p\tau_p} \left[\mu_n\tau_n\bar{p} \int_{E_v}^{E_c} Nf\tau dE + \mu_p\tau_p\bar{n} \int_{E_v}^{E_c} N(1-f)\tau dE \right]}{\bar{n} \int_{E_v}^{E_c} (1-f)(\bar{p} + e_p)\tau NdE \left(\bar{p} \int_{E_v}^{E_c} Nf\tau dE \right) + \int_{E_v}^{E_c} \bar{p}f(\bar{n} + e_n)\tau NdE \left(\bar{n} \int_{E_v}^{E_c} N(1-f)\tau dE \right)} \frac{\mu_n\bar{n} + \mu_p\bar{p}}{G}, \quad (49)$$

which can also be transformed, according to Eq. (15), into

$$\frac{I_{ac}}{I} = \gamma \frac{G_{ac}}{G}, \quad (50)$$

where I is the dc current due to the steady flux of light illuminating the sample.

The above expression closely resembles the usual expression defining γ [see Eq. (13)] where δG and δI have been replaced by G_{ac} and I_{ac} , respectively. This means that, rather than working under dc conditions and varying the dc flux to measure γ , one can also work with a small ac signal superposed to the dc one, make the frequency very low, and use the ratio of the ac to dc components to calculate γ , and eventually to achieve a DOS spectroscopy.

As a conclusion of this section, it is clear that all the mentioned techniques are intimately linked, though each of them, taken separately, brings some precise information on the DOS parameters. In this paper, the results of these techniques (SSPC, MPC-HF, MPC-LF, SSPG) will be compared via numerical simulations to underline the information that can be extracted from a comparison of the various data.

C. Summary

Before presenting simulation details and results, let us first summarize what is known directly from the different techniques presented above.

The MPC-LF technique brings the value of $N(E_{fn})$ from the generation rate, the temperature, and the slope of the tangent of the phase shift ϕ measured at low frequencies, following the equation⁵

$$N(E_{fn}) = \frac{2G \tan(\phi)}{k_B T \omega}. \quad (51)$$

The energy scaling uses the same equation as for the γ spectroscopy [Eq. (28)] and thus requires the knowledge of $\mu_n N_c$.

The MPC-HF technique gives the quantity NC/μ from experimentally known parameters as, for instance, the ac generation rate G_{ac} and the modulus of the resulting ac photocurrent I_{ac} , according to the equation¹⁹

$$\frac{N(E_\omega)C_n}{\mu_n} = \frac{2}{\pi k_B T} Sq\xi G_{ac} \frac{\sin \phi}{|I_{ac}|}. \quad (52)$$

The C_n involved in the MPC-HF- NC/μ is that of the probed states, but a proper energy scaling requires the knowledge of the quantity $C_n N_c$, also called the attempt-to-escape frequency, since E_ω follows from

$$E_c - E_\omega = k_B T \ln \left(\frac{C_n N_c}{\omega} \right). \quad (53)$$

From the γ measurements by SSPC we obtain the $\gamma - NC/\mu$ values directly from experimental quantities like the generation rate, the photoconductivity and γ [see Eq. (27)]. However, the proper energy scaling requires the knowledge of the quantity $\mu_n N_c$. In these $\gamma - NC/\mu$ values, the C involved is that of the centers providing the main recombination path, or an average value of the capture coefficients of the states involved in the recombination path [see Eq. (33)]. The results of the SSPC measurements made under dc illumination can be cross checked with those of photoconductivity measurements performed in ac or with data extracted from the SSPG technique.

V. SIMULATIONS

We have developed computer codes to check the calculations and the links between the different photoconductivity techniques exposed above. Actually, two simulations codes were developed independently, both in Argentina and in France, using different software. We have thus the possibility to cross-check the results of each of them.²⁰ In these simulations, various DOS distributions can be introduced in the gap of a semiconductor. All the parameters of the considered semiconductor—such as, for instance, gap width, extended-states mobilities of the carriers, equivalent densities of states at the band edges, capture coefficients of the defects for electrons and holes—can be defined by the user, as well as the “experimental” parameters such as light flux, temperature range, and temperature steps. Since the continuity and charge neutrality equations are solved, the occupancy of the states is fully determined. At a given temperature the simulation calculates the photoconductivity values σ_1 and σ_2 , for a given flux F_1 and for $F_2 = F_1 \times 1.1$ respectively, by solving numerically the continuity and charge neutrality equations. The γ value is deduced from the photoconductivities at these two fluxes as

$$\gamma = \frac{F_1}{\delta F} \frac{\delta \sigma}{\sigma_1},$$

with $\delta F = F_2 - F_1$ and $\delta \sigma = \sigma_2 - \sigma_1$. Then, by using Eq. (27) the $\gamma - NC/\mu$ distribution is obtained depending only on experimental parameters such as G , σ , T , and γ . The simulation calculates also the ac current resulting from a modulated excitation at different frequencies and hence what would be the MPC-LF or MPC-HF results. Finally, the simulation can calculate the β values obtained when two beams of fluxes F_1

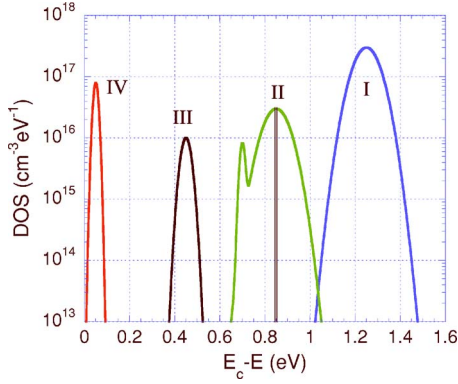


FIG. 2. (Color online) Typical density of states introduced in the simulations to represent a crystalline semiconductor.

and $F_1/10$ are interfering with a grating period ranging from 0.15 to 108 μm . Then it calculates the $\beta\text{-}NC/\mu$ distribution from Eq. (41) applied to simulated SSPG results obtained with a grating period of 108 μm . For some simulations we will compare the $\gamma\text{-}NC/\mu$ and $\beta\text{-}NC/\mu$ distributions to validate the calculations presented in Sec. IV A.

We want to underline that the simulations were not developed to fit any experimental results but rather to understand the processes involved in the experiments. The “materials” we have studied were either crystalline materials with rather narrow distributions of defects or amorphous materials exhibiting broad distributions of defects. For each material, we have studied both the rather unrealistic case of a single species of defect and a case including at least two species of states. For a-Si:H the case of amphoteric states has also been studied.

A. Crystalline semiconductors

We have defined an imaginary crystalline semiconductor whose DOS is presented in Fig. 2. Four defect distributions have been introduced in the 1.8 eV wide band gap of the material. All these distributions are Gaussian shaped except the one in the middle of the gap (Type II states), which was chosen unsymmetrical for reasons explained below. States of type I are centered at $E_c - E_{maxI} = 1.25$ eV and are donor states; states of type II have a maximum positioned at $E_c - E_{maxII} = 0.85$ eV and are acceptor states; states of type III are centered at $E_c - E_{maxIII} = 0.45$ eV and are also acceptor states; and states of type IV are made of a narrow distribution of donors

states close to the conduction band edge. This small quantity of donor states has been added so that the electrical neutrality under dark equilibrium leads to a dark Fermi level pinned close to the middle of the gap (double vertical line, $E_c - E_{f0} = 0.85$ eV). We want to stress that these donor states are too close to the conduction band to have any influence on the behavior of the material under illumination, except at extremely high fluxes out of the range that we used in our simulations. Under these conditions the material is very slightly n type. The predominance of electrons in the transport has been reinforced choosing an extended-states mobility of 10 $\text{cm}^2 \text{V}^{-1} \text{s}^{-1}$ for the electrons and of 1 $\text{cm}^2 \text{V}^{-1} \text{s}^{-1}$ for the holes. According to the developments presented in the previous sections, we expect then to obtain a major contribution of the electrons to the photocurrent. However, note that the defect distribution around the Fermi level has been chosen unsymmetrical, so that it will be easier to estimate if the simulated photoconductivity techniques are probing the states above or below the dark Fermi level, which is the electrons or holes DOS, respectively. Other characteristics of the defect states (maximum density, capture coefficients) are summarized in Table I.

Various simulations were performed to test the reliability of the calculations exposed in the previous sections. The SSPC technique was simulated for temperatures in the range 130–350 K, varied in 10 K steps, with a flux $F_1 = 10^8 \text{ cm}^{-2} \text{ s}^{-1}$ ($G_1 = 1.3 \times 10^{12} \text{ cm}^{-3} \text{ s}^{-1}$). The SSPG technique was simulated in the same range of temperatures and with the same flux. The MPC-HF experiment was simulated with the same flux in a temperature range 200–380 K in 20 K steps, with frequencies of the modulation in the range 1 Hz–5 kHz.

1. One species of states

We have first studied a “crystal” containing a single species of states. All the capture coefficients were taken identical for all the states: $C_n = 2 \times 10^{-8} \text{ cm}^3 \text{ s}^{-1}$ for the electrons and $C_p = 10^{-8} \text{ cm}^3 \text{ s}^{-1}$ for the holes. We present in Fig. 3 the NC/μ spectroscopies obtained from the simulations of the SSPC ($\gamma\text{-}NC/\mu$, open squares), of the SSPG ($\beta\text{-}NC/\mu$, open stars) and of the MPC-HF (dashed lines). The NC/μ distributions obtained from these different techniques are compared to the NC/μ that we have introduced in the simulation (full lines).

It can be seen in Fig. 3 that the agreement between the various NC/μ distributions calculated from SSPC, SSPG,

TABLE I. Summary of the parameters of the DOS used in the various simulations illustrating the crystalline semiconductor case. W is the standard deviation of the Gaussian defect distributions. The hole capture coefficient was the same for all the states, $C_p = 10^{-8} \text{ cm}^3 \text{ s}^{-1}$.

	$E_c - E_{max}$ (eV)	N_{max} ($\text{cm}^{-3} \text{ eV}^{-1}$)	W (meV)	Same C_n ($\text{cm}^3 \text{ s}^{-1}$)	Different C_n ($\text{cm}^3 \text{ s}^{-1}$)
States I	1.25	3×10^{17}	50	2×10^{-8}	2×10^{-9}
States II	0.85	3×10^{16}	50	2×10^{-8}	2×10^{-8}
	0.7	8×10^{15}	10	2×10^{-8}	2×10^{-8}
States III	0.45	1×10^{16}	20	2×10^{-8}	2×10^{-8}

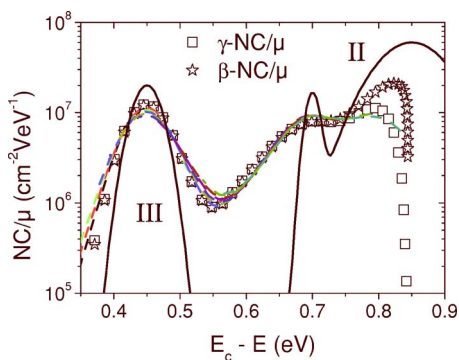


FIG. 3. (Color online) NC/μ distributions obtained from SSPC (open squares), SSPG (open stars), and MPC-HF (dashed lines) compared to the NC/μ distributions introduced in the simulation (full lines).

and MPC-HF is excellent. The various defect peaks introduced in the simulation are also rather well revealed. The material parameters have been chosen such that the transport is dominated by electrons, so it is the DOS between the dark Fermi level and the conduction band edge that is probed by the different techniques. However, one can see that the experimental NC/μ distributions are slightly wider and present maxima slightly lower than the introduced ones. This behavior is probably due to the narrowness of the probed peaks. Indeed, for all the techniques simulated here, the final equations giving the possibility to achieve a DOS spectroscopy are the results of approximations. For instance, if one considers the SSPC method, the quantity $N(E_m)$ has been extracted from an integral in which the normalizing term [$e_n \tau^2(E)$, see Eq. (21)] is a peaked function exponentially decreasing with slopes $\pm 1/k_B T$ at both sides of the maximum value, located at $E_m \approx E_{fn}$. At high temperatures this peaked function is rather wide and, in the present case, wider than the probed peaks. The result is that, compared to the “real” peaks, the obtained peaks are smoothed by the approximation shown in Eq. (21). The same type of approximation holds for the SSPG and MPC-HF methods, leading to the same type of smoothing. It can also be seen that the energy range of the γ - NC/μ and β - NC/μ distributions is limited to $E_c - E \leq 0.85$ eV. At this limiting value, which corresponds to the position of the dark Fermi level, both distributions drop. Indeed, at high temperatures, where the deepest states are probed, the splitting of the quasi-Fermi levels is small and, consequently, one has $E_{fn} \approx E_{f0}$.

Considering the type III states at 0.45 eV from E_c , the agreement between the γ - NC/μ and the MPC-HF- NC/μ distributions is such that they present their maximum at the same energy. Of course, the energy scaling for both distributions was done knowing the values of $\mu_n N_c$ (γ - NC/μ) and $C_n N_c$ (MPC-HF- NC/μ). Under true experimental conditions, where these parameters are often unknown, the adjustment of the maxima obtained with each technique for a given peak of defects could lead to the determination of the ratio C_n/μ_n , giving information both on the defect parameters (C_n) and on the material parameters (μ_n).

2. Different species of states

The above case where all the capture coefficients are identical is highly unrealistic. That is why we have per-

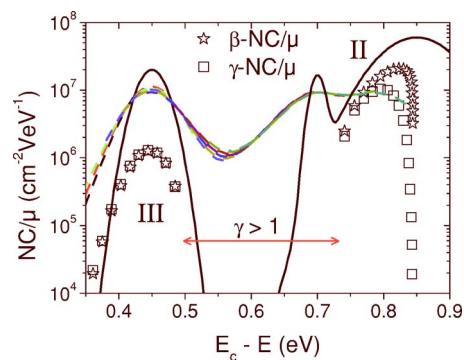


FIG. 4. (Color online) Comparison of the NC/μ distributions obtained from SSPC (open squares), SSPG (open stars), and MPC-HF (dashed lines) with the introduced NC/μ (full lines) for the case where the type I states have an electron capture coefficient ten times lower than the other states. The energy range for which we obtain $\gamma > 1$ is indicated on the figure.

formed simulations for which the electron capture coefficient of state I was chosen to be ten times lower than that of the other states (see Table I). We present in Fig. 4 the NC/μ distributions obtained from SSPC, SSPG, and MPC-HF, and we compare them to the introduced NC/μ . The various experimental parameters (e.g., flux, temperature range) were taken the same as in the above case with a single species of states.

It can be clearly seen in Fig. 3 that the MPC-HF- NC/μ distribution is the same as in the case of a single species of states. As mentioned early in Sec. IV C, the reason for this behavior is that the MPC-HF technique is only sensitive to the capture coefficients of the probed states. On the contrary, though we observe an excellent agreement between the γ - NC/μ and β - NC/μ distributions, they are far from reproducing the actual NC/μ . At high energies (i.e., at high temperatures), the two distributions are almost identical to what we have obtained with a single type of states; but with decreasing temperature there is a range of energies where the DOS cannot be reproduced simply because we have $\gamma > 1$, leading to unrealistic negative NC/μ values when one uses Eq. (27). When the temperature is further decreased, the shape of type III states is rather well reproduced, but with values a factor of 10 below what we have obtained from MPC-HF.

The fact that γ is found larger than 1 in a given temperature range can be explained in the framework of the model proposed by Rose to explain the sensitization observed in some semiconductors.¹² According to the Rose model, the sensitization results from the presence in the gap of the semiconductor of two species of states: one around the middle of the gap with a high electronic capture cross section and a low density of states, and another one close to the valence band with a lower electronic capture coefficient and a high density of states. In the case presented above the defect characteristics have been chosen according to this model: the electron capture coefficient of states II and III is ten times higher than the electron capture coefficient of states I, whereas the density of states I is ten times higher than that of states II.

We present in Fig. 5 the evolution with the light flux F of the ratio σ/F (which is proportional to the lifetime), where σ

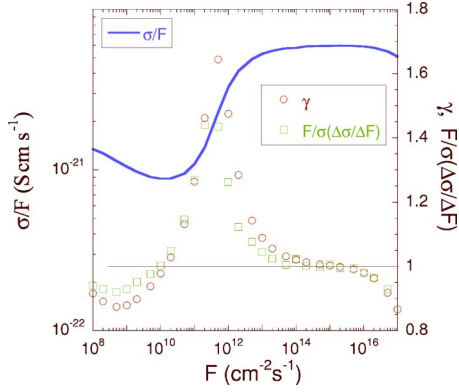


FIG. 5. (Color online) Evolution of the ratio σ/F of the sample with the “applied” flux (full line). Evolutions of γ as well as $(F/\sigma)(\Delta\sigma/\Delta F)$ are also shown. The horizontal line indicates when these two quantities are equal to 1.

is the photoconductivity of the sample. One can see that there is a sudden rise of σ/F for F in the range 10^{11} – 10^{13} $\text{cm}^{-2} \text{s}^{-1}$, which also corresponds to a peak in the γ value (calculated as $\gamma = (F/\sigma)(\delta\sigma/\delta F)$). For comparison we have also calculated $(F/\sigma)(\Delta\sigma/\Delta F)$, where ΔF is the difference between two successive fluxes in the 1-2-5 series that we have used in the simulation ($F = 10^8, 2 \times 10^8, 5 \times 10^8, \dots, \text{cm}^{-2} \text{s}^{-1}$). As can be seen, though the evolutions of γ and $(F/\sigma)(\Delta\sigma/\Delta F)$ are similar, the calculated values of this last quantity are certainly highly dependent on the ΔF used, especially when σ is varying rapidly with F . Thus, experimentally, γ should be determined as it was in the simulation, that is, calculating $(F/\sigma)(\delta\sigma/\delta F)$ using small values of δF —such as, for instance, 10–20% of the total flux. We can add that, according to Eq. (15), γ may depend on G . Thus, the coefficient γ defined as usual from $\sigma \propto G^\gamma$, and calculated by plotting the variations of σ with a generation rate varying sometimes over decades, has very little connection with the local γ coefficient that we use in this paper.

One interesting point is that there exists a range of fluxes where the ratio σ/F (i.e., the electron lifetime) suddenly rises, corresponding to values of γ much larger than one. It means that, by introducing a DOS that gives the material all the characteristics of a “sensitizable” one, as defined by Rose, we actually reproduce the behavior of the majority carrier’s lifetime predicted by the Rose model. At low fluxes only the central peak of defects II plays a major role in the recombination of carriers. The coefficient γ is smaller than 1 and decreases slightly with increasing flux. For higher values of the flux the splitting of the quasi-Fermi levels is such that states I start to participate in the recombination. The simulation also clearly shows that, as predicted by the model, the larger capture coefficient for electrons of states II causes an electron transfer from state I to states II until these latter are almost completely filled. Thus, progressively the recombination path shifts from states II, with a high capture coefficient, to states I, with a lower capture cross section, resulting in an increase of the electron lifetime and hence of the photoconductivity with increasing flux. For the highest flux, only states I plays a role in the recombination, and the photoconductivity and γ resume their “regular” behavior with increasing flux (e.g., $\gamma < 1$).

The material we have defined is thus sensitizable, and the behavior observed in Fig. 5 with increasing flux at a fixed temperature can also be observed with a decreasing temperature at a given flux. That is why at high temperatures the γ - NC/μ and β - NC/μ behaviors shown in Fig. 4 are the same as if there were a single species of state, since recombination is controlled by states II. As temperature is decreased, the recombination path shifts progressively from states II to states I and this sensitization process results in γ values larger than 1. With further decrease of temperature, the recombination is fully controlled by states I and one finds again γ values lower than 1.

The fact that at low temperatures the γ - NC/μ and β - NC/μ distributions are a factor of 10 below the MPC-HF- NC/μ distribution can be explained in the following way. If we neglect the holes contribution, from Eq. (33) we have

$$\frac{1}{\gamma} - 1 = \frac{N_n^{III}}{\frac{1}{C_n^I \tau_n^I} + \frac{1}{C_n^{II} \tau_n^{II}} + \frac{1}{C_n^{III} \tau_n^{III}}} = \frac{C_n^{III} N_n^{III}}{\frac{10}{\tau_n^I} + \frac{1}{\tau_n^{II}} + \frac{1}{\tau_n^{III}}}, \quad (54)$$

where N_n^I and N_n^{II} have been omitted since in the probed region, close to the quasi-Fermi level for electrons, these two values are negligible. In the considered temperature range, γ is lower than 1 because the recombination is almost completely controlled by the states of class I, as it is the case in the high flux range shown in Fig. 5. Thus, the dominant term in the denominator of Eq. (54) is the first one, the electron lifetime being almost equal to τ_n^I ($\tau_n \approx \tau_n^I$). We can finally write

$$\frac{1}{\gamma} - 1 = \frac{C_n^{III} \tau_n^I N_n^{III}}{10} = \frac{C_n^{III} \tau_n N_n^{III}}{10}. \quad (55)$$

Thus, when one plots γ - NC/μ , one ends with values ten times lower than they should be, as shown in Fig. 4.

We want to stress here that the agreement we have in Fig. 4 is essentially due to the fact that we have assumed the existence of a dominant recombination center. For a real crystal this may not be the case, and thus one would determine an “average” density of states [see Eq. (33)] that could be different from the “true” density of states. This is one of the reasons why the results of this analysis should be taken cautiously if the technique is experimentally used alone, with no comparison with some other methods.

We have also studied the influence of the position in the gap of states I. Using the same parameters as above we have performed simulations for which the position of states I was pushed upwards towards the valence band edge. The energy position of the maximum of these states was increased from $E_c - E_{MaxI} = 1.25$ eV to 1.35 eV, 1.45 eV, and 1.6 eV. We present in Fig. 6 the evolution of the different γ - NC/μ distributions obtained with the various $E_c - E_{MaxI}$. It can be seen that the energy (i.e., the temperature) corresponding to the onset of $\gamma > 1$ decreases when $E_c - E_{MaxI}$ increases. This behavior can be explained by the fact that the sensitization process starts when the quasi-Fermi levels splitting is such that states I begins to play a role in the recombination. With increasing $E_c - E_{MaxI}$ the splitting of the quasi-Fermi levels must be increased, that is, the temperature lowered, for states

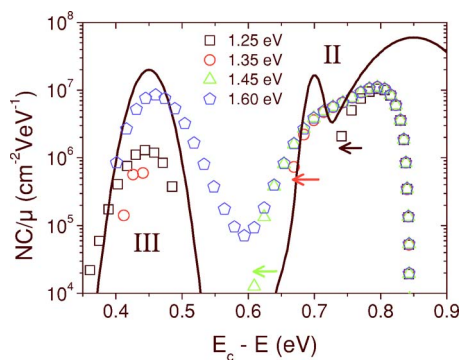


FIG. 6. (Color online) Evolution of the γ - NC/μ distribution with the position in the gap of the type I states. The arrows indicate the onset of $\gamma > 1$.

I to start playing a role in the recombination process. It can be even seen that with $E_c - E_{MaxI} = 1.6$ eV the recombination is always controlled by states II, so that the γ - NC/μ distribution obtained is the same as if there were a single species of state in the gap. In this case, states I are too close to the valence band edge to be reached by the holes' quasi-Fermi level in the range of temperatures we have used. These simulations show that, to obtain an efficient sensitization, in addition to the introduction of states with different capture coefficients and different densities, the relative position of the states in the gap is also of some importance.

To conclude with this part we may add that, as in the case of a single species of state, provided that for a true material γ is not always larger than 1 in the temperature range of the experiment, it is possible to extract some parameters of the defects and of the material combining the SSPC and the MPC-HF experiments. The adjustment of the peak energy position measured by both techniques can lead to the determination of the ratio C_n/μ_n between the capture coefficients of the states and the extended-states mobility. In addition, the ratio between two peaks maxima, each one being measured by a different technique, may give an order of magnitude of the ratio between the capture coefficients of the states and the capture coefficient of the recombining states. We will see below that in the case of a-Si:H, for which no well-defined peak exists, three techniques are needed to extract the same information.

B. The case of a-Si:H

First, we will consider an “ideal” material with only one species of states. Then we will consider the case of materials

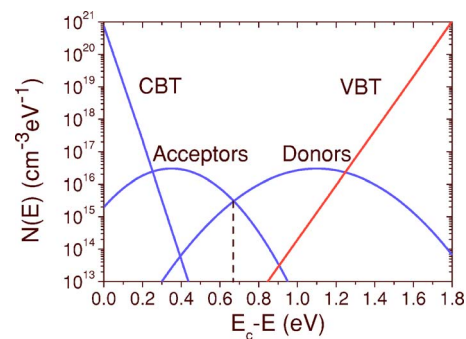


FIG. 7. (Color online) Typical density of states for an a-Si:H-like material that we have used in our simulations. The dark Fermi level is indicated by a dashed vertical line.

presenting different species of states, and we will finish by taking into account the presence of amphoteric states.

1. One species of states

We present in Fig. 7 a rather typical density of states for a-Si:H. The mobility gap was fixed at 1.8 eV, and the characteristic temperatures of the band tails were taken equal to $T_c = 275$ K and $T_v = 600$ K for the conduction and valence band tails, respectively. These values were chosen according to the values of the characteristic temperatures or of the Urbach energy found in the literature for device grade films.^{21,22} The equivalent density of states at the band edges were taken equal to the values for crystalline silicon: $N_c = N_v = 2.5 \times 10^{19}$ cm⁻³ at $T = 300$ K and varied as $T^{3/2}$. These values give densities of states at the band edges equal to 10^{21} cm⁻³ eV⁻¹.²³ The deep states were taken as two Gaussian distributions, one of acceptor states located at $E_c - E = 0.35$ eV, with a standard deviation of 0.15 eV and a maximum value of 3×10^{16} cm⁻³ eV⁻¹, and another one of donor states located at $E_c - E = 1.1$ eV, with a standard deviation of 0.2 eV and the same maximum value. These two distributions pin the dark Fermi level at $E_c - E_{f0} = 0.67$ eV and are such that the total concentration of deep states is of the order of 2.5×10^{16} cm⁻³, in agreement with deep defect densities quoted in the literature.²² The following capture coefficients have been assumed for all the states: $C_p = 10^{-8}$ cm³ s⁻¹ and $C_n = 2 \times 10^{-8}$ cm³ s⁻¹ (Table II, third row). This last value was proposed to be the capture coefficient of the conduction band tail states from simulations of the time-of-flight experiment.²⁴ The electron and hole mobilities were chosen

TABLE II. Summary of the different capture coefficients used in the various simulations for a-Si:H.

	CBT		VBT		Donor		Acceptor	
	C_n^H (cm ³ s ⁻¹)	C_p^H (cm ³ s ⁻¹)	C_n^I (cm ³ s ⁻¹)	C_p^I (cm ³ s ⁻¹)	C_n^d (cm ³ s ⁻¹)	C_p^d (cm ³ s ⁻¹)	C_n^a (cm ³ s ⁻¹)	C_p^a (cm ³ s ⁻¹)
Same C	2×10^{-8}	10^{-8}						
$C_n^I = C_n^H/10$	2×10^{-8}	10^{-8}	2×10^{-9}	10^{-8}	2×10^{-8}	10^{-8}	2×10^{-8}	10^{-8}
$R=2$	2×10^{-8}	10^{-8}	2×10^{-9}	10^{-8}	10^{-8}	10^{-8}	2×10^{-8}	5×10^{-9}
$R=10$	2×10^{-8}	10^{-8}	2×10^{-9}	10^{-8}	2×10^{-9}	10^{-8}	2×10^{-8}	10^{-9}
$R=50$	2×10^{-8}	10^{-8}	2×10^{-9}	10^{-8}	4×10^{-10}	10^{-8}	2×10^{-8}	2×10^{-10}

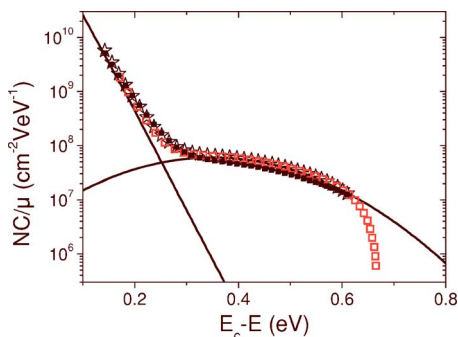


FIG. 8. (Color online) Reconstruction of $\gamma NC/\mu$ by means of Eq. (27) (open symbols). The NC/μ distribution measured by MPC in the low frequency domain is also shown (full squares). They can be compared to the NC/μ introduced in the simulation (lines).

equal to $\mu_n=10 \text{ cm}^2 \text{ V}^{-1} \text{ s}^{-1}$ and $\mu_p=1 \text{ cm}^2 \text{ V}^{-1} \text{ s}^{-1}$, respectively, according to time-of-flight results,²¹ though higher values of the order of $30 \text{ cm}^2 \text{ V}^{-1} \text{ s}^{-1}$ have also been proposed for the electron extended-states mobility.²⁴

We present in Fig. 8 the $\gamma NC/\mu$ distribution reconstructed by means of Eq. (27) (open symbols) in which we have introduced the calculated γ values. This $\gamma NC/\mu$ curve can be compared to the introduced NC/μ distribution (lines). Note that the energy scaling is referred to as E_c since, being the electrons the majority carriers in a-Si:H, it is the quantity $E_c - E_{fn}$, determined from photoconductivity, that gives the energy scaling [Eq. (28)]. The calculation was made for temperatures varying from 90 K to 450 K in 10 K steps, and with two generation rates of $6.5 \times 10^{19} \text{ cm}^{-3} \text{ s}^{-1}$ (stars) and $6.5 \times 10^{17} \text{ cm}^{-3} \text{ s}^{-1}$ [open squares (\square)]. It is clear that the NC/μ reconstruction is particularly accurate. It can also be seen that the $\gamma NC/\mu$ deviates from the true NC/μ in the vicinity of the energy position of the dark Fermi level E_{f0} , a behavior that we were expecting since the lower limit of $E_c - E_{fn}$ is precisely $E_c - E_{f0}$. In Fig. 8 we also plot the NC/μ distribution that could be deduced from MPC-LF measurements [full squares (\blacksquare)], using for the ratio C/μ the electron capture coefficient of the CBT, C_n^{CBT} , and the electron extended-states mobility, μ_n . As expected, taking into account the calculation results presented in Sec. IV B, the agreement between the MPC-LF- NC/μ , the $\gamma NC/\mu$, and the NC/μ introduced in the simulation is excellent. We have not presented either the results of the $\beta NC/\mu$ or those of the MPC-HF- NC/μ to lighten the figure but, of course, the agreements with the other techniques and the actual NC/μ are also excellent.

Note that in this peculiar case of a single species of state we do not observe any quenching of the photoconductivity, contrarily to what is often observed in a-Si:H. Figure 9 shows an Arrhenius plot of the photoconductivity for the two generation rates. It can be seen that the photoconductivity steadily increases with temperature, though there is clearly a temperature range where the increase of σ with temperature slows down compared to the two other regions, at high and low temperatures, where σ increases rapidly. In this temperature range, the γ values approach 1, although they remain lower than 1. From the experimental point of view, this situation might cause some troubles, since a small error in the

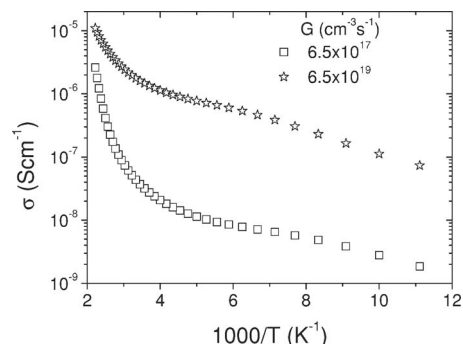


FIG. 9. Arrhenius plot of the calculated photoconductivities for two generation rates, where no quenching can be seen.

determination of γ can lead to a large error in the DOS [see Eq. (27)]. Thus, in this case, extra care should be taken for a correct experimental determination of γ .

2. Different species of states

We have performed another simulation introducing into the calculation the same DOS as the one presented in Fig. 7. However, we have modified the electron capture coefficient of the valence band tail, which has been reduced by a factor of 10. Thus, we are dealing with two species of states: class I, the valence band tail states, for which $C_n^I=2 \times 10^{-9} \text{ cm}^3 \text{ s}^{-1}$ and $C_p^I=10^{-8} \text{ cm}^3 \text{ s}^{-1}$, and class II, all the other states, for which $C_n^{II}=2 \times 10^{-8} \text{ cm}^3 \text{ s}^{-1}$ and $C_p^{II}=10^{-8} \text{ cm}^3 \text{ s}^{-1}$ (Table II, fourth row). The other parameters were kept identical to the ones used in Sec. V B 1, except that we made all the calculations with a generation rate of $6.5 \times 10^{18} \text{ cm}^{-3} \text{ s}^{-1}$, in between those used in Sec. V B 1.

Figure 10 presents the Arrhenius plot of the calculated photoconductivity σ . A clear quenching of σ can be seen, approximately in the same temperature range where it is found experimentally.¹⁵ From this curve we expect to have γ values larger than 1, leading to unreasonable negative DOS values when using the reconstruction based on Eq. (27). Of course, this situation sets a limitation to the SSPC technique, which cannot be applied to reconstruct the DOS in this temperature range.

We have also calculated the evolution of the photoconductivity and γ for different values of the VBT characteristic

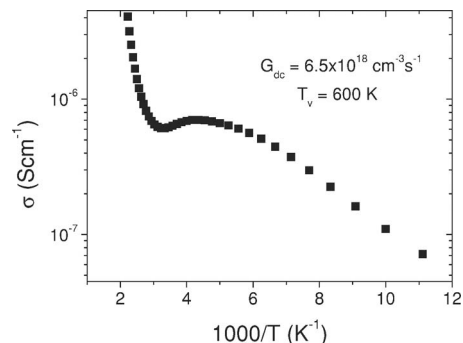


FIG. 10. Arrhenius plot of the calculated photoconductivity. A quenching of σ appears in the temperature range $240 \text{ K} \leq T \leq 320 \text{ K}$.

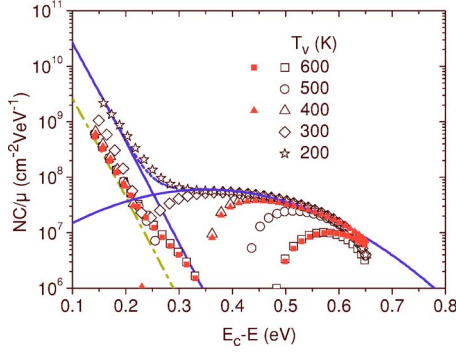


FIG. 11. (Color online) γ - NC/μ reconstructed by means of Eq. (27) from the results of our simulations (symbols) compared to the introduced NC/μ (full lines). The dashed line represents the sum of the conduction band tail and the deep states. The dash-dotted line shows the NC/μ of the CBT divided by a factor of 10. The γ - NC/μ have been calculated for different characteristic temperatures of the valence band tail indicated in the figure. β - NC/μ distributions (full symbols) calculated for two T_v values are also displayed to be compared with the γ - NC/μ ones.

temperature to explore a range such as $200 \text{ K} \leq T_v \leq 600 \text{ K}$. The reconstruction of γ - NC/μ using Eq. (27) is shown in Fig. 11. In the high-energy range, the fit with the introduced NC/μ depends on the characteristic temperature T_v of the valence band tail: the lower T_v , the better the fit. With decreasing energy a gap appears, due to the quenching of the photoconductivity leading to negative γ - NC/μ values ($\gamma > 1$). At low energies, the γ - NC/μ reproduces well the shape of the conduction band tail (CBT), but with values approximately ten times lower than the true NC/μ of the introduced band tail for $T_v \geq 400 \text{ K}$. A departure from the previous γ - NC/μ curves occurs for $T_v = 300 \text{ K}$, and finally for $T_v = 200 \text{ K}$ the reconstructed γ - NC/μ matches the introduced NC/μ values of the CBT.

In the cases of high T_v values ($T_v \geq 400 \text{ K}$), the behavior at shallow energies (low temperatures) can be explained as in Sec. V A 2. If we neglect the holes' contribution, from Eq. (33) we have

$$\frac{1}{\gamma} - 1 = \frac{N_n^{II}}{\frac{1}{C_n^I \tau_n^I} + \frac{1}{C_n^{II} \tau_n^{II}}} = \frac{C_n^{II} N_n^{II}}{\frac{10}{\tau_n^I} + \frac{1}{\tau_n^{II}}}, \quad (56)$$

where N_n^I has been omitted, since it is linked to the exponentially decreasing VBT density taken at the quasi-Fermi level for electrons. Taking the peculiar shape of the DOS into account, i.e., a large VBT and a narrow CBT, the integral of the states between the quasi-Fermi levels for state I (VBT) is much higher than the same integral for state II. It means that $1/\tau_n^I$ is much larger than $1/\tau_n^{II}$, so that the lifetime is $\tau_n \approx \tau_n^I$ and we can finally write

$$\frac{1}{\gamma} - 1 = \frac{C_n^{II} \tau_n^I N_n^{II}}{10} = \frac{C_n^{II} \tau_n N_n^{II}}{10} = C_n^I \tau_n N_n^{II}. \quad (57)$$

Thus, the γ - NC/μ values take account of a capture coefficient $C_n^I = C_n^{II}/10$ instead of C_n^{II} , and one ends with a distri-

bution ten times lower than the actual one. This is exactly what is shown in Fig. 11, where the γ - NC/μ distribution at shallow energies (low T) parallels the CBT- NC/μ roughly a factor of 10 below it.

At high temperatures Eq. (33) is still valid. Nevertheless, the quasi-Fermi levels are much closer to midgap and, taking the peculiar shape of the DOS into account, the integral of the states between the quasi-Fermi levels for state I is much lower—the valence band tail is exponentially decreasing—than the same integral for state II. It means that $1/\tau_n^I$ is much smaller than $1/\tau_n^{II}$, so that the lifetime is $\tau_n \approx \tau_n^{II}$ and we can finally write

$$\frac{1}{\gamma} - 1 = C_n^{II} \tau_n N_n^{II}. \quad (58)$$

Thus, the capture coefficient implicitly involved in the γ - NC/μ values is C_n^{II} , and one ends with a γ - NC/μ not far from the real NC/μ . This is exactly what is observed in Fig. 11, where the symbols at high energies (high T) match the actual NC/μ .

Between these two temperature ranges there is an intermediate range for which N_p^I and/or N_p^{II} are much higher than N_n^{II} , simply because the CBT decreases much faster than the VBT. At low temperatures, both quasi-Fermi levels are located within the tail regions. An increasing temperature reduces the energy difference between the quasi-Fermi levels, and E_m rapidly reaches the deep states whereas E_{tp}^I is still in the valence band tail. Thus, the large ratio between the N_p and N_n may compensate the small ratio between \bar{p} and \bar{n} , and it is the negative term of Eq. (32), the second addend in the numerator, that takes the place over the positive term leading to γ values larger than 1.

Note also that the temperature—or energy—range in which γ is larger than 1 depends on the characteristic temperature of the valence band tail. This is due to the fact that a narrow valence band tail (e.g., $T_v = 400 \text{ K}$) is reached by the quasi-Fermi level for trapped holes at a lower temperature than a wider band tail ($T_v = 600 \text{ K}$). The evolution of the threshold temperature is therefore identical to the one seen in Sec. V A 2, when we moved states of class I closer to the valence band. Actually, the valence band tail is playing the role of states of class I whereas the conduction band tail is playing the role of states of class II. This process explains why, with $T_v = 600 \text{ K}$, the γ - NC/μ does not reproduce the introduced NC/μ , even at high energies, simply because the threshold temperature is high and the corresponding energies close to the Fermi level: γ tends to be larger than 1 at rather high temperatures.

In this context—shift of the threshold temperature towards low values with the decrease of T_v —it may seem strange that for $T_v = 300 \text{ K}$ and 200 K we never obtain $\gamma > 1$, and even, with $T_v = 200 \text{ K}$ the γ - NC/μ distribution is almost perfectly following the CBT- NC/μ one. Actually, this behavior can also be explained within the Rose model, in which the deeper states with the lower C_n (Class I) are also supposed to be much more numerous than the class II states. This assumption is of fundamental importance, since it is needed that the states of class II are completely filled by

electrons coming from states of class I, so that the recombination path shifts from one species of states to the other with the consequent increase of the electron lifetime. If the characteristic temperature of the VBT is not very different from that of the CBT, then there are not enough electrons coming from the VBT states to fill the CBT ones. Thus, there is no shift of the recombination path and experimentally everything appears as if there were a single species of states, the CBT states, which are consequently well reproduced by the reconstructed $\gamma NC/\mu$ distribution. This means that, contrarily to what was said by Tran,¹⁵ the mechanism that results in γ values larger than 1 is the same described in the Rose model, which seems to perfectly apply to a-Si:H.

In order to check the validity of the calculation of Sec. IV A we have also simulated SSPG experiments for the two cases $T_v=600$ K and $T_v=400$ K. The $\beta NC/\mu$ distributions deduced from the simulation are shown in Fig. 11 with full symbols. The agreement with the $\gamma NC/\mu$ distributions calculated from photoconductivity simulations is excellent except in a very small energy range close to the dark Fermi level.

Finally, thus far, the parameters used in the simulations were rather limited, and one can wonder about the possibility of extracting DOS parameters from a real experiment when the deep states are made of amphoteric states. In this case, different capture coefficients for the neutral and charged states need to be taken into account.

That is why, before showing simulations on amphoteric states, we would like to show some results obtained when different capture coefficients are assumed for the deep states. In addition to the lower electron capture coefficient of the VBT states compared to the CBT states of the previous case, in these simulations we also assume that the electron capture coefficient of the donor states, C_n^d , is lower than the electron capture coefficient of the acceptor states, C_n^a , and that the hole capture coefficient of the acceptor states, C_p^a , is lower than the hole capture coefficient of the donor states, C_p^d , by the same ratio R as for the electrons. Thus we have $C_n^d = C_n^a/R$ and $C_p^a = C_p^d/R$, where we have given R the values $R=2, 10, \text{ and } 50$. The various capture coefficients used in the simulations for a-Si:H are summarized in Table II.

The reconstructed $\gamma NC/\mu$ distributions, calculated with a generation rate of $6.5 \times 10^{18} \text{ cm}^{-3} \text{ s}^{-1}$, are shown in Fig. 12(a) and compared to the introduced NC/μ . It can be seen that at low temperatures (shallow states) the $\gamma NC/\mu$ distributions parallel the CBT with a value approximately ten times lower, exactly as in the previous case and for the same reasons, whereas for the deep states, close to the dark Fermi level ($E_c - E \approx 0.6$ eV), the ratio of the introduced NC/μ to the reconstructed $\gamma NC/\mu$ roughly equals the ratio R between the capture coefficients. This behavior is again due to the fact that the C involved in the $\gamma NC/\mu$ distribution is not that of the probed states, as it is the case for the MPC-HF measurements, but that of the dominant recombination states. Though the density ratio between the acceptor and donor states is not high, the donor states are more numerous than the acceptor states because of a larger standard deviation of its Gaussian distribution (see Fig. 7). This difference is enough for the recombination path to be predominantly via the donor states that present a lower electron capture cross

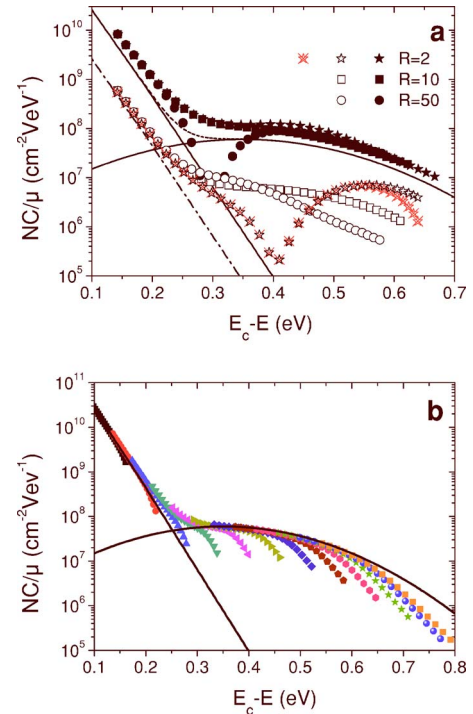


FIG. 12. (Color online) (a) Comparison of the various $\gamma NC/\mu$ calculated with different R (open symbols) with the NC/μ introduced in the simulation. The MPC-LF- NC/μ distributions calculated for the different ratios are also shown as full symbols. A $\beta NC/\mu$ distribution (crossed stars) calculated for $R=2$ is also displayed, to be compared with the $\gamma NC/\mu$ one. The dashed line represents the sum of the conduction band tail and the deep states. The dash-dotted line shows the NC/μ of the CBT in which C is the C_n of the valence band tail. (b) The calculated MPC-HF- NC/μ distribution fits rather well the NC/μ introduced in the simulation.

section than the acceptor states. Hence, the C involved in the $\gamma NC/\mu$ is that of the donor states and not that of the probed acceptor states.

In between these two energy ranges one has to consider that the valence band tail starts to play a role in the recombination and that this intervention probably leads to the gap that appears in the $\gamma NC/\mu$ curve calculated with $R=2$. In this energy range one can hardly deduce any interesting information on the DOS parameters.

As a matter of illustration we also present in Fig. 12(a) results of a SSPG simulation performed in the case $R=2$ (crossed stars). It can be seen that, as in Fig. 11, the $\beta NC/\mu$ and the $\gamma NC/\mu$ distributions are identical except close to the dark Fermi level.

In Fig. 12(a) we have also plotted the results of the reconstruction from the MPC-LF technique (full symbols). We recall that this technique only provides the $N(E_{fn})$ values, so we have used the ratio C_n^{CBT}/μ_n to plot this MPC-LF- NC/μ . It can be seen that, as far as the CBT is concerned, the agreement between the CBT- NC/μ and the MPC-LF- NC/μ is rather good, here within a factor of 1.5. This is also the case for the deep states close to the Fermi level, where a rather good agreement is also found whatever the value of R . The slight differences in energy position of the MPC-LF- and $\gamma NC/\mu$ are due to the fact that the energy position of the

γ - NC/μ points comes from the true position of E_{fn} whereas that of the MPC-LF points is deduced from the photoconductivity, thus including the very small holes contribution (see, for instance, the right-hand side of the two curves with stars). Note that the DOS deduced from the slope of $\tan(\phi)$ in the MPC-LF technique can be negative (here in the case $R=50$). This behavior results in the gap that appears around $E_c - E = 0.3$ eV in the MPC-LF- NC/μ curve. Though we have no theoretical interpretation at present, this behavior is a clear signature of the presence of various species of states, whose influence on the charge transport intermixes at a given temperature range. In Fig. 12(b) we show the results of the calculation of the MPC-HF- NC/μ , and it can be seen that the agreement with the NC/μ introduced in the simulation is also nice both for the CBT and the deep states.

3. The case of amphoteric states

The nature and origin of the deep defect density in a-Si:H has been a matter of debate for years. A consensus was found on the fact that dangling bonds (DB) were at the origin of the deep states. However, the fact that these states are amphoteric, being positive if no electron is present (D^+), neutral if one electron occupies the state (D^0) and negative if two electrons are trapped (D^-), raised the question of the statistics to be used—of course, different from the well-known Fermi-Dirac that we have used above—and also of the sign of the correlation energy U , which is the energy difference between the singly and doubly occupied states.^{25,26} It is now almost generally agreed that in chalcogenides U is negative²⁷ and that in a-Si:H U is positive with a value between 0.2 and 0.4 eV.^{28,29} Further, a model of formation of these dangling bonds based on thermodynamical considerations was proposed.^{30,31} This defect-pool model was then formalized by Deane and Powell.^{32,33}

In our simulation software, it is possible to introduce the parameters of a defect-pool distribution of defects. The proper statistics for correlated states is used to solve the continuity and charge neutrality equations, so that the occupation functions of the different states and species of states are completely calculated. In a previous paper we had shown that the states occupancy could be rather complicated,³ but whatever the occupancy we can calculate the photoconductivity for different temperatures and/or fluxes, deduce a γ - NC/μ distribution by means of Eq. (27), and compare it to the introduced NC/μ as we did in the previous examples.

We present in Fig. 13 the density of states that we have used. The band tails and their capture coefficients were taken identical to that of the last two cases studied: $C_n^I = C_n^{II}/10$. The pool parameters were the following: the hydrogen concentration was taken equal to $[H] = 5 \times 10^{21} \text{ cm}^{-3}$, the pool position was located at $E_c - E_{pool} = 0.5$ eV, the standard deviation was $\sigma_{pool} = 0.2$ eV, the correlation energy $U = 0.3$ eV, the equilibration temperature $T_{eq} = 450$ K, and the number of bonds created by the weak-bond/DB conversion process was taken equal to 2. With these parameters, the dark Fermi level was pinned at $E_c - E_{f0} = 0.8$ eV and the D^0 integrated density was equal to $2.7 \times 10^{16} \text{ cm}^{-3}$. The capture coefficients for the charged DB were fixed at $C_n^+ = C_p^- = 3 \times 10^{-8} \text{ cm}^3 \text{ s}^{-1}$, and the capture coefficients of the neutral DB ($C_n^0 = C_p^0$) were taken R

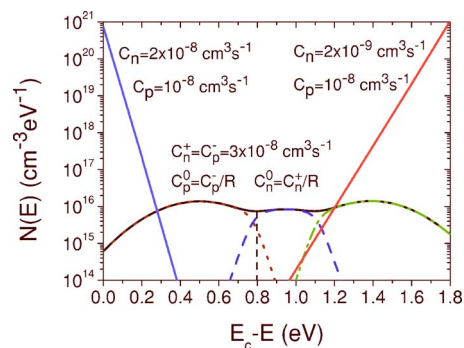


FIG. 13. (Color online) Density of states including a defect-pool distribution of deep defects. The D^+ distribution is shown in dotted line, the D^0 is shown in dashed line, the D^- by the dash-dotted line. The envelope is represented by the full line. The energy position of the dark Fermi level is shown by a vertical dashed line.

times lower, with $R=2, 10$, or 50 . The γ - NC/μ calculated for the different ratios R and with a generation rate of $6.5 \times 10^{18} \text{ cm}^{-3} \text{ s}^{-1}$ are presented in Fig. 14, where they are compared to the NC/μ defined in the simulation.

The similarity of the γ - NC/μ curves shown in Fig. 14 with those presented in Fig. 12 is striking. Again, as for all the simulations in which we have chosen to take $C_n^I = C_n^{II}/10$, we observe that at low energies the γ - NC/μ curve parallels the CBT- NC/μ distribution with values ten times lower. The “universality” of this property is not surprising if we consider that these points are obtained at low temperatures and/or high fluxes. Under these conditions the nature of the deep defects (monovalent or DB) and their capture coefficients have no influence at all on the recombination path. Taking into account the exponential variation with energy of the conduction and valence band tails, under high fluxes or low temperatures only these states are involved in the recombination process. Consequently, only two species of states need to be considered and the Rose model applies perfectly well.

Note also the excellent agreement between the MPC-LF- NC/μ and the CBT- NC/μ for all the simulations if one uses,

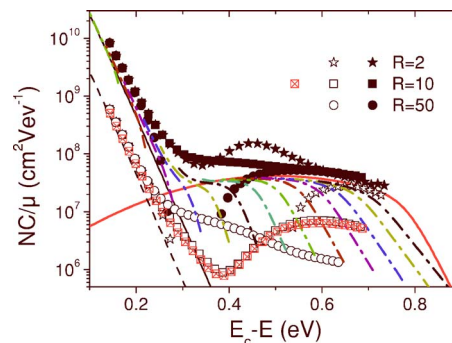


FIG. 14. (Color online) γ - NC/μ distributions (open symbols) and MPC-LF- NC/μ (full symbols) obtained for different ratios of the charged to neutral DB capture coefficients, compared to the NC/μ introduced in the simulation (full lines). The dash-dotted lines represent the MPC-HF- NC/μ distribution. A β - NC/μ distribution (crossed squares) calculated for $R=10$ is also displayed to be compared with the γ - NC/μ one. The dashed line shows the NC/μ of the CBT in which C is the C_n of the valence band tail.

as we did, the capture coefficient of the CBT states to reconstruct the MPC-LF- NC/μ . The reason for this behavior is the same as above. At high fluxes or low temperatures, only two types of states have to be considered, the CBT and the VBT states. We have shown in a previous paper² that, if electrons are the majority carriers as is usually the case in a-Si:H, the MPC-LF technique is probing the DOS interacting with them, which is the CBT in our case.

As far as the deep states are concerned one can see that, considering the states close to the dark Fermi level and within a factor of 1.5, the ratio of the actual NC/μ to the $\gamma NC/\mu$ is equal to the ratio $R=C_n^+/C_n^0$, in a similar way to what we had found for the deep monovalent states of the preceding case. Of course, this behavior is linked to the same reasons as those exposed above. Actually, it is worth noting that the ratio R can also be estimated from the ratio between the MPC-LF- NC/μ distribution and the $\gamma NC/\mu$ one.

Finally, we have simulated a SSPG experiment and deduced a $\beta NC/\mu$ distribution for $R=10$ that fits quite well with the $\gamma NC/\mu$ distribution calculated from the photoconductivity simulation. As a conclusion, we can see that even in the case of amphoteric states the behavior of the different techniques can be predicted as in the case of monovalent states.

4. Experimental determination of some parameters of the material

As for the case of a crystalline material, for all the simulations performed above the energy scaling of the curves was achieved according to the introduced values of the capture coefficient of the CBT and of the electron extended-states mobility. Experimentally these quantities are unknown. However, we can propose a method to determine a good order of magnitude of these quantities. Indeed, at low temperatures we have shown that only the CBT states are probed by the MPC-LF and MPC-HF techniques whatever the nature of the deep states. In this low-temperature range, remember that the MPC-HF technique gives the values of NC/μ with an energy scaling linked to C_n^{CBT} , whereas the MPC-LF gives the N values with an energy scaling depending on μ_n . Hence, the adjustment of the MPC-LF- NC/μ to the MPC-HF- NC/μ by tuning the C_n^{CBT} and μ_n values should lead to some rather precise knowledge of these two parameters. In addition, having this μ_n value, one obtains the en-

ergy scaling for the $\gamma NC/\mu$ distribution. Consequently, one can deduce the values of the capture coefficients of the recombining states, such as the valence band tail states at low temperatures and the deep states at high temperatures, by the ratio between the $\gamma NC/\mu$ and the MPC-LF- NC/μ distributions. We will show this procedure applied both to crystalline and amorphous samples in the article that follows this one.

VI. CONCLUSION

In conclusion, we have theoretically examined the dependence of the steady-state photoconductivity on the light intensity, providing an analytical expression for the coefficient γ that describes this dependence. When a single species of defect states is present in the gap of the semiconductor, we have shown that a very simple formula relating the DOS at the electron quasi-Fermi level to the γ coefficient can be obtained. When different species of traps are present, we have shown that the γ coefficient can be larger than 1, a phenomenon called superlinearity, observed for different materials at low temperatures. Applying further simplifications we have examined what information on the DOS can be extracted from measurements of the γ coefficient as a function of temperature and light flux.

We have theoretically demonstrated a close connection between the γ -DOS and two other methods used for DOS estimation: the modulated photocurrent performed in both regimes (high and low frequencies) and the steady-state photocarrier grating technique. We have shown that the association of MPC-HF, MPC-LF, and γ measurements can lead to the evaluation of several DOS parameters that could not be obtained with the methods taken individually. Both in the case of a crystalline “material” and of an a-Si:H “film” we have proposed a method to determine experimentally some unknown parameters, such as, for instance, the capture cross section of the conduction band tail and the extended-states mobility. In the case of a-Si:H, one can even obtain the capture coefficient of the deep states or of the valence band tail states by a close comparison between the results of various photoconductivity experiments.

ACKNOWLEDGMENTS

This work was partially supported by PEI No. 6329 from CONICET and Project No. A02E01 from Ecos Sud-SECyT.

¹H. Oheda, J. Appl. Phys. **52**, 6693 (1981).

²C. Longeaud and J. P. Kleider, Phys. Rev. B **45**, 11672 (1992).

³C. Longeaud and J. P. Kleider, Phys. Rev. B **48**, 8715 (1993).

⁴R. R. Koropeccki, J. A. Schmidt, and R. Arce, J. Appl. Phys. **91**, 8965 (2002).

⁵M. E. Gueunier, C. Longeaud, and J. P. Kleider, Eur. Phys. J.: Appl. Phys. **26**, 75 (2004).

⁶D. Ritter, E. Zeldov, and K. Weiser, Appl. Phys. Lett. **49**, 791 (1986).

⁷I. Balberg, R. Naidis, L. F. Fonseca, S. Z. Weisz, J. P. Conde, P.

Alpuim, and V. Chu, Phys. Rev. B **63**, 113201 (2001).

⁸I. Balberg, J. Non-Cryst. Solids **299-302**, 531 (2002).

⁹I. Balberg, Y. Dover, R. Naidis, J. P. Conde, and V. Chu, Phys. Rev. B **69**, 035203 (2004).

¹⁰J. A. Schmidt and C. Longeaud, Appl. Phys. Lett. **85**, 4412 (2004).

¹¹J. A. Schmidt and C. Longeaud, Phys. Rev. B **71**, 125208 (2005).

¹²A. Rose, *Concepts in Photoconductivity and Allied Problems* (Wiley & Sons, New York, 1966).

¹³J. Z. Liu and S. Wagner, Phys. Rev. B **39**, 11156 (1989).

- ¹⁴D. Mendoza and W. Pickin, *Phys. Rev. B* **40**, 3914 (1989).
- ¹⁵M. Q. Tran, *Philos. Mag. B* **72**, 35 (1995).
- ¹⁶D. S. Shen and S. Wagner, *J. Appl. Phys.* **78**, 278 (1995).
- ¹⁷J. G. Simmons and G. W. Taylor, *Phys. Rev. B* **4**, 502 (1972).
- ¹⁸G. W. Taylor and J. G. Simmons, *J. Non-Cryst. Solids* **8-10**, 940 (1972).
- ¹⁹J. P. Kleider and C. Longeaud, *Solid State Phenomena*, edited by H. Neber-Aeschbacher (Scitec Publications Ltd., 1995), pp. 597–646.
- ²⁰One simulation (DEOST) is available on the web at www.lgep.supelec.fr/scm
- ²¹T. Tiedje, in *Semiconductors and Semimetals 21C*, edited by J. Pankove (Academic Press, New York, 1984), pp. 207–238.
- ²²M. Stutzmann, *Philos. Mag. B* **60**, 531 (1989).
- ²³K. Winner and L. Ley, in *Amorphous Semiconductors and Related Materials*, edited by H. Fritzsche (World Scientific, Singapore, 1989), p. 365.
- ²⁴R. Vanderhaghen, *Phys. Rev. B* **38**, 10755 (1988).
- ²⁵D. Adler and E. J. Yoffa, *Phys. Rev. Lett.* **36**, 1197 (1976).
- ²⁶H. Okamoto and Y. Hamakawa, *Solid State Commun.* **24**, 23 (1977).
- ²⁷G. J. Adriaenssens, *Philos. Mag. B* **62**, 79 (1990).
- ²⁸D. Adler, *Phys. Lett.* **41**, 1755 (1978).
- ²⁹J. K. Lee and E. A. Schiff, *Phys. Rev. Lett.* **68**, 2972 (1992).
- ³⁰K. Winer, *Phys. Rev. B* **41**, 12150 (1990).
- ³¹G. Schumm and G. H. Bauer, *Philos. Mag. B* **64**, 515 (1991).
- ³²S. C. Deane and M. J. Powell, *Phys. Rev. Lett.* **70**, 1654 (1993).
- ³³M. J. Powell and S. C. Deane, *Phys. Rev. B* **48**, 10815 (1993).